# CryoEM reveals unprecedented binding site for $Na_V1.7$ inhibitors enabling rational design of potent hybrid inhibitors

Marc Kschonsak[1*], Christine C. Jao[1*], Christopher P. Arthur[1], Alexis L. Rohou[1], Philippe Bergeron[2], Daniel F. Ortwine[2], Steven J. McKerrall[2], David H. Hackos[3], Lunbin Deng[3], Jun Chen[4], Peter S. Dragovich[2], Matthew Volgraf[2], Matthew R. Wright[5], Jian Payandeh[1,#], Claudio Ciferri[1,#], John C. Tellis[2,#]

[1]Genentech Inc., Structural Biology; South San Francisco, CA, United States.
[2]Genentech Inc., Discovery Chemistry; South San Francisco, CA, United States.
[3]Genentech Inc., Neuroscience; South San Francisco, CA, United States.
[4]Genentech Inc., Biochemical and Cellular Pharmacology; South San Francisco, CA, United States.
[5]Genentech Inc., Drug Metabolism and Pharmacokinetics; South San Francisco, CA, United States.

[#]Corresponding authors. Email: jpayandeh@exelixis.com (J.P); ciferri.claudio@gene.com (C.C.); tellis.john@gene.com (J.C.T.).

**Author Contributions:** J.P., C.C., and J.C.T. designed research, M.K., C.J., C.P.A., A.R., D.H., and J.C., performed research, J.C.T, P.B., D.O., S.M., P.S.D., and M.V. analyzed data and contributed to compound design. J.C.T., C.C., J.P., and M.K. wrote the paper.

**Competing Interest Statement:** M.K., C.C.J, A.L.R, D.F.O, D.H.H, L.D, J.C, P.S.D, M.W, C.C and J.C.T are Genentech employees. All authors declare no competing financial interest.

## Abstract

The voltage-gated sodium ($Na_V$) channel $Na_V1.7$ has been identified as a potential novel pain target due to its striking human genetics. However, clinically available drugs (e.g. lidocaine, carbamazepine, etc.) are not selective among the nine $Na_V$ channel subtypes, $Na_V1.1$-$Na_V1.9$, and the two currently known classes of $Na_V1.7$ subtype-selective inhibitors (aryl- and acylsulfonamides) have undesirable characteristics that may limit their development. Moreover, understanding of the structure-activity relationships of the acylsulfonamide class of $Na_V1.7$ inhibitors, exemplified by the clinical development candidate **GDC-0310**, has been based solely on a single co-crystal structure of an arylsulfonamide inhibitor series. To advance inhibitor design targeting the $Na_V1.7$ channel, we established an iterative system to routinely obtain high-resolution ligand-bound $Na_V1.7$ structures using cryogenic electron microscopy (cryo-EM). We report that **GDC-0310** engages the $Na_V1.7$ voltage-sensing domain 4 (VSD4) through an unexpected binding mode orthogonal to the arylsulfonamide class binding pose, which identifies a previously unknown ligand binding site in $Na_V$ channels. This finding enabled the design of a novel hybrid inhibitor series that bridges the aryl and acylsulfonamide binding pockets and allows for the generation of molecules with substantially differentiated structures and properties. Overall, this study highlights the power of cryo-EM methods to pursue challenging drug targets using iterative and high-resolution structure-guided inhibitor design. It also underscores an important role of the membrane bilayer in the discovery of selective $Na_V$ channel modulators.

## Introduction

Voltage-gated sodium ($Na_V$) channels initiate and propagate action potentials in excitable tissues and play important roles in health and disease.[1,2] The $Na_V1.7$ channel is expressed predominantly in the peripheral nervous system and genetic studies have identified compelling loss-of-function and gain-of-function phenotypes in human pain syndromes, prompting significant efforts to develop $Na_V1.7$-selective inhibitors as potential novel analgesic drugs.[3-5] $Na_V$ channels contain 24-transmembrane segments linked in four homologous domains (DI-DIV), where four peripheral voltage-sensor domains (VSD1-4) surround a central ion-conducting pore module that houses the ion selectivity filter and key ligand and toxin receptor sites. Traditionally, all clinically available $Na_V$ channel inhibitors lack significant molecular selectivity among the $Na_V1.1$–$1.9$ subtypes owing to the high sequence conservation found at the ligand binding site within the central cavity of the ion conducting pore module.[5,6]

A breakthrough study in 2013 by McCormack and colleagues reported the discovery of an arylsulfonamide antagonist, **PF-04856264**, that bound to an unprecedented receptor site in VSD4 with demonstrated molecular selectivity for human $Na_V1.7$ over other subtypes.[7] However, the related development candidate **PF-05089771** did not meet clinical endpoints in human subjects with painful diabetic peripheral neuropathy, possibly due to poor target coverage and the intolerable doses required to achieve efficacy.[8-10] Additionally, an alternate acylsulfonamide inhibitor that also

79 targeted the VSD4 receptor site in $Na_V1.7$, **GDC-0276**, was halted in Phase I clinical
80 trials due to safety concerns and potential off-target effects likely attributed to the high
81 lipophilicity of the compound.[11,12] To date, selective $Na_V1.7$ inhibitors with an improved
82 therapeutic index relative to these clinical-stage compounds have not yet been identified,
83 and this absence underscores the need to optimize such molecules using modern,
84 structure-guided design approaches.
85
86 The inherent complexity and dynamic nature of human $Na_V$ channels have
87 historically presented significant barriers to obtaining high-resolution experimental
88 structural information, especially of inhibitor-bound complexes.[13] Using an engineered
89 human VSD4 $Na_V1.7$-$Na_VAb$ bacterial channel chimera and X-ray crystallography, the
90 binding mode of the **GX-936** arylsulfonamide inhibitor (Supplementary Figure 1)
91 revealed that the anionic sulfonamide group engages the fourth arginine gating charge
92 (R4) to trap VSD4 in an activated conformation, which stabilizes a non-conductive,
93 inactivated state of the channel.[14] While determinants of subtype selectivity and
94 structure-activity relationships (SAR) of the arylsulfonamide inhibitor class could be
95 rationalized by the **GX-936** co-crystal structure, additional ligand-bound structures of
96 suitable resolution were not returned by the $Na_V1.7$-$Na_VAb$ chimeric channel
97 crystallography system. This shortcoming led molecular docking studies to presume that
98 the acylsulfonamide inhibitors also bound VSD4 in an analogous manner, despite points
99 of inexplicable SAR.[15] The overall paucity of direct structural information has made the
100 optimization of $Na_V1.7$ inhibitors challenging, with many questions about the
101 determinants of potency, selectivity, and the relationship between the acylsulfonamide
102 and arylsulfonamide inhibitor classes remaining unanswered.
103
104 Over the last three decades, protein crystallography and structure-based drug
105 design (SBDD) have become gold standards across the pharmaceutical industry for the
106 identification of ligand binding pockets and the optimization of drug candidates for
107 clinical development. While SBDD has proven successful for many important targets,
108 including G protein-coupled receptors (GPCRs),[16] its applicability to several membrane
109 protein targets, such as $Na_V$ channels, has been limited due to the extreme difficulties
110 with their iterative crystallization and structure determination.[13] Cryogenic electron
111 microscopy (cryo-EM) has recently emerged as a transformative technique to determine
112 the high-resolution structures of diverse protein targets and has proven particularly
113 effective for membrane proteins that are recalcitrant to crystallization.[17] Despite this
114 breakthrough, cryo-EM structure determination of membrane targets in complex with
115 small or large molecule therapeutics frequently remains retrospective and is often enabled
116 after the advancement of key molecules into the clinic.[18,19] Sluggish turn-around times
117 and modest resolutions typically afforded by cryo-EM have limited its application for
118 real-time SBDD efforts. Here, we describe a system for the iterative determination of
119 high-resolution $Na_V1.7$ small molecule co-structures via cryo-EM that has led to the
120 development of a novel class of inhibitors. Critical to this advancement has been
121 establishment of a robust protocol for sample preparation and structure determination and
122 the enablement of the first structure of an acylsulfonamide bound to $Na_V1.7$ VSD4,
123 revealing a previously unknown pocket between the S3 and S4 helices. Consequently, a
124 novel hybrid inhibitor series bridging the aryl and acylsulfonamide pockets was

generated. Our work exemplifies the deployment of cryo-EM as a workhorse structural biology tool in an active medicinal chemistry campaign and thus represents an important milestone toward $Na_V$ channel drug discovery.

## Results

### Structure of the G-3565-VSD4 $Na_V1.7$-$Na_VPas$ channel complex in lipid nanodiscs

Our approach to establish an iterative, high-resolution system to enable $Na_V1.7$ SBDD was ultimately guided by three observations: our repeated failure to generate well-diffracting crystals of the $Na_V1.7$-$Na_VAb$ bacterial channel chimera system,[14] our difficulty of reproducibly expressing a suitable amount of full-length human $Na_V1.7$ channel,[20,21] and the very limited local resolution observed at VSD4 in all available human Nav1.7 cryo-EM structures.[22,23] Thus, we sought to exploit an engineered human VSD4-$Na_V1.7$-$Na_VPas$ cockroach channel chimeric construct that had been previously shown to complex with small molecule inhibitors and peptide toxins known to target VSD4.[21] The robust protein yields following expression and purification allowed us to readily pursue reconstitution of the VSD4-$Na_V1.7$-$Na_VPas$ channel into lipid nanodisc with high recovery (Supplementary Figure 2). Small molecule inhibitors were added prior to sample vitrification, followed by cryo-EM data collection and processing procedures, which allowed us to routinely obtain 3D-reconstructions in the 2.2-3.0 Å resolution range (Figure 1, Supplementary Figure 3).

The VSD4-$Na_V1.7$-$Na_VPas$ chimera displays the expected domain-swapped arrangement with numerous densities assigned as phospholipids bound to the channel, confirming the maintenance of a native membrane-like environment (Figure 1). As seen in previous $Na_VPas$ structures,[21,24,25] the ion-conducting pore module of the VSD4-$Na_V1.7$-$Na_VPas$ chimeric channel is closed, consistent with a nonconductive or inactivated state. The quality and resolution of our structure allowed us to assign 112 water molecules for the highest resolution structure (Figure 1, Video 1). The visualization of many well-resolved water molecules bound within the VSDs and coordinated within the ion selectivity filter provides new insights into the interactions that might occur during gating charge transfer and ion conduction, respectively.

Although we were able to determine the crystal structure of VSD4-$Na_VAb$ bound to the arylsulfonamide inhibitor **GX-936**,[14] no well-diffracting crystals were obtained for any other arylsulfonamide compounds despite years of continued effort. Arylsulfonamide **GNE-3565** is representative of an advanced series of arylsulfonamide class $Na_V1.7$ inhibitors that demonstrates channel blockage at subnanomolar concentrations with mixed subtype selectivity (Figure 2A). We complexed **GNE-3565** with the VSD4 $Na_V1.7$-$Na_VPas$ channel-nanodisc system and employed cryo-EM to assess its overall binding pose (Figure 2B, C). The 2.9 Å resolution cryo-EM map revealed that the S1-S2 and S3-S4 helices from VSD4 form a clamshell-like structure that closes over **GNE-3565** (Figure 2D, E, Supplementary Data Figure 4A-D, Supplementary Data Table 1), similar to the binding pose reported for **GX-936**.[14] Specifically, the ionized arylsulfonamide group of **GNE-3565** (measured pKa = 5.8) bisects VSD4 to salt-bridge directly to R4 on

171 the S4 helix, while the central phenyl ring extends perpendicular between the S2 and S3
172 helices to directly contact established subtype-selectivity determinants Tyr1537 and
173 Trp1538 on the S2 helix (Figure 2A-D). As for **GX-936**, the **GNE-3565** arylsulfonamide
174 VSD4 receptor binding site can be divided into three regions: an anion-binding pocket, a
175 selectivity pocket, and a lipid-exposed pocket (Figure 2D). The root-mean-square
176 deviation (RMSD) between the **GNE-3565**-VSD4 and the **GX-936**-VSD4 structures[14] is
177 0.667 (714 to 714 atoms), (Supplementary Figure 5A), supporting long-held assumptions
178 by medicinal chemistry teams that all structurally-related arylsulfonamides should be
179 expected to complex to VSD4 through similar determinants.[8,26-31]
180
181 **Structure of the acylsulfonamide GDC-0310 in complex with the VSD4 $Na_V$1.7-**
182 **$Na_V$Pas channel**
183 To investigate the binding pose of a representative $Na_V$1.7 selective
184 acylsulfonamide, **GDC-0310** (Figure 3A) was complexed with the VSD4 $Na_V$1.7-$Na_V$Pas
185 channel in nanodiscs and a cryo-EM structure was determined to 2.5 Å resolution (Figure
186 3B-D, Supplementary Data Figure 3G-J, Supplementary Data Table 1). Remarkably, the
187 binding mode of **GDC-0310** revealed an unexpected and previously unknown pocket that
188 formed between the S3 and S4 helices (Figure 3B-E). While the aryl and acyl moieties of
189 **GDC-0310** and **GNE-3565** bind in the same region, the remainder of the acyl receptor
190 site is orthogonal to the corresponding binding domain reported for the aryl class (Figure
191 3B-D). In detail, the anionic acylsulfonamide of **GDC-0310** participates in salt-bridge
192 bonding interactions with R4 and R3 through the carbonyl and sulfonamide oxygen
193 atoms, respectively (Figure 3F). Moreover, the aryl ring of the **GDC-0310** splits the S3
194 and S4 helices to occupy a lipophilic pocket, displacing the S3 helix laterally by ~3 Å
195 relative to the **GNE-3565**-VSD4 structure (Figure 3G). Our cryo-EM inhibitor bound
196 structures serve to highlight a dynamic environment in VSD4 where the S1-S4 helixes
197 can be differentially separated by distinct small molecule binding poses (Figure 2D,
198 Figure 3D).
199
200 It is notable that the cyclopropyl substituent of **GDC-0310** makes effective van
201 der Waals interactions with I1574 and I1588 from S3 and I1601 and I1604 on S4 (Figure
202 3G), while the alpha-methylbenzylamine "tail" region sits almost entirely within the lipid
203 bilayer (Figure 3A, C), where density for this portion of the inhibitor is only poorly
204 resolved (Figure 3E). Considering the relative depth of the **GDC-0310** binding site in
205 relation to the membrane-water interface (~8 Å), our structure suggest a membrane
206 access pathway for acylsulfonamides to the VSD4 receptor site, which has important
207 implications for understanding the pharmacology, SAR, and potential development
208 liabilities of the series.[32] Notably, this structure also reveals that the Tyr1537 side-chain
209 on S2 exists in a down rotamer and does not contact **GDC-0310** directly, which provides
210 the first direct structural rationale for why the selectivity profiles between the acyl and
211 arylsulfonamide classes differ substantially (Figure 3D, *vide infra*).[33]
212
213 **Structure-based rational design of hybrid $Na_V$1.7 inhibitors**
214 Upon inspection of the superimposed **GNE-3565**-aryl and **GDC-0310**-acyl
215 structures, we could immediately envision a novel class of hybrid inhibitors that would
216 simultaneously occupy both the aryl- and acylsulfonamide binding pockets (Figure 4A,

217 B). Such an enlarged hybrid binding pocket would offer unique opportunities to gain
218 potency directly from ligand-protein interactions, which might enable removal of the
219 hydrophobic lipid-facing tail groups seen in all previous generations of VSD4-targeting
220 $Na_V$ channel inhibitors. These groups have typically been critical for maintaining
221 potency, but use of the plasma membrane to drive membrane-bound target occupancy is
222 largely nonspecific, and potentially introduces off-target liabilities that can contribute to
223 toxicity. However, it was unclear if this hybrid conformation of the VSD4 domain could
224 accommodate the described inhibitors and/or whether it was accessible during any stage
225 of $Na_V1.7$ channel activation. We therefore set out to demonstrate proof-of-concept that
226 appropriately designed small molecules could induce this hypothesized receptor state
227 while inhibiting channel function with meaningful potency.
228
229 **GDC-0310** was a relatively unattractive starting point for hybridization because
230 of its high molecular weight (543 g/mol) and lipophilicity (cLogP = 5.2). Accordingly,
231 analysis of historical data identified progenitor compound **1**, which offers reasonable
232 potency against $Na_V1.7$ ($IC_{50}$ = 25 nM, n = 8; Fig 4C) and reduced molecular weight (350
233 g/mol) and lipophilicity (cLogP = 2.7). Seeking to leverage existing knowledge of the
234 arylsulfonamide binding pocket, molecule **2** was synthesized in an attempt to directly
235 graft on a significant portion of the **GNE-3565** scaffold. Gratifyingly, this molecule
236 retained substantial potency, affording channel blockade at an $IC_{50}$ of 47 nM (n = 8).
237
238 A cryo-EM structure of **2** bound to the VSD4 $Na_V1.7$-$Na_VPas$ channel confirmed
239 that the molecule adopts the desired hybrid binding mode (Figure 4D). Here, the anionic
240 group of the novel hybrid compound binds in the same position as in the aryl and acyl
241 poses, interacting closely with R4, as seen for the aryl-like binding (Figure 4E). The aryl-
242 and acylsulfonamide-derived structural motifs of **2** occupy their expected positions in the
243 pockets formed between S2/S3 and S3/S4, respectively. Notably, in this hybrid
244 configuration, Y1537 adopts a similar arrangement as observed for the arylsulfonamides
245 (Figure 4F).
246
247 Encouraged by this result, we hoped to draw on previously established knowledge
248 of acylsulfonamide SAR to improve the potency of this compound. Established SAR
249 within the acylsulfonamide series suggested that replacement of the chloro substituent on
250 the benzamide fragment of the molecule with a cyclopropane would typically improve
251 potency. This SAR proved translatable to the hybrid class molecules, resulting in
252 inhibitor **3** ($IC_{50}$ = 16 nM, n = 12; Figure 4C).
253
254 Further analysis of the cryo-EM structure of **2** revealed that the aryl ring in the
255 S2/S3 binding pocket was shifted ~1 Å away from the VSD4 core when compared to
256 arylsulfonamides such as **GNE-3565** (data not shown). The aryl ring in the S3/S4 pocket
257 exhibited better overlap with the analogous substituents in the **GDC-0310** structure. We
258 hypothesized that the acylsulfonamide moiety of **2**, which places the two aryl substituents
259 4.7 Å apart, might not be fully optimized for use in hybrid inhibitors. In comparison, an
260 arylsulfonamide moiety would position these two groups at a distance of ~3.3 Å. On this
261 basis we designed *N*-benzothiazolyl sulfonamide **4**, which demonstrated potent $Na_V1.7$
262 inhibition ($IC_{50}$ = 9 nM, n = 8, Figure 4C).

Our last hypothesis was again validated with a cryo-EM co-structure of **4** bound to the VSD4 $Na_V1.7$-$Na_VPas$ channel (Figure 4G). Here, we observed the typical face-on pi-stacking orientation of the S2/S3 substituent with Y1537 while maintaining efficient space filling in the S3/S4 pocket. Moreover, the efficient occupation of the non-membrane exposed regions of the binding pocket permitted the removal of the lipophilic tail of the molecule in **5**, where a $CF_3$ group replaces the cyclopentylmethyl substituent. Although this molecule shows reduced potency ($IC_{50}$ = 74 nM, n = 8), lack of substantial small molecule contact with the lipid bilayer is an uncommon feature in all other known $Na_V1.7$ VSD4 domain inhibitors. These molecules serve as a key proof of concept, highlighting the power of cryoEM to yield new structural insights that can inspire the design of novel, structurally differentiated small molecule inhibitors.

## Discussion

Iterative structure-based design is among the most powerful techniques to facilitate the development of small molecule drug candidates. Although a variety of technologies are capable of providing information about small molecule ligand-protein interactions, SBDD has traditionally been synonymous with the use of X-ray crystallography, with other techniques failing to rival its high resolution and fast cycle times. Here, we have demonstrated that a robust cryo-EM structure pipeline is sufficient to quickly provide co-structures at resolutions suitable for use in an active medicinal chemistry optimization campaign. Moreover, we have highlighted the power of structural methods, and cryo-EM in particular, to provide new and important insights into inhibitor design through the discovery of a previously unknown binding mode for acylsulfonamide $Na_V1.7$ inhibitors. We further note that our use of an engineered VSD4-$Na_V1.7$-$Na_VPas$ chimeric channel construct was essential to produce high yields of recombinant protein capable of routinely returning multiple cryo-EM samples per preparation. This system repeatedly delivered high-resolution depictions of the VSD4 inhibitor binding site and thus strongly contrasts with all prior accounts of cryo-EM structures of full-length human $Na_V1.7$ channels.[22,23] Importantly, high quality cryo-EM maps at VSD4 in complex with ICA121431 have recently been reported from full-length human $Na_V1.3$ channel protein,[37] indicating that SBDD efforts targeting a particular $Na_V$ channel subtype would benefit from exploring both engineered and native channel sample options at early project stages.

The co-structure of **GDC-0310** was critical to contextualize historical differences between aryl- and acylsulfonamide $Na_V1.7$ inhibitors, which include divergent SAR in the linker phenyl ring and tail regions, disparate $Na_V$ family selectivity patterns, and differences in on-rates and off-rates.[12,15,33-36] Previous efforts to model acylsulfonamide binding have attempted to dock molecules into the **GX-936** co-structure and have proposed subtle changes in molecular register and/or pose to explain the non-translatable SAR.[15,38] Here, we demonstrate that the molecular features of aryl- and acylsulfonamide inhibitors diverge because they occupy distinct, but overlapping, pockets within the VSD4 domain.

The selectivity determinants of arylsulfonamide $Na_V1.7$ inhibitors have been well studied. Mutation of key non-conserved residues proximal to the binding pocket observed in the **GX-936** co-structure have been shown to alter $Na_V1.7$ potency consistent with selectivity patterns observed for other $Na_V$ family members.[14] Typically, arylsulfonamides have shown high levels of selectivity against $Na_V1.5$, $Na_V1.1$, and $Na_V1.4$, but lower selectivity against $Na_V1.2$ and $Na_V1.6$. In comparison, several acylsulfonamides have been characterized with very high selectivity over $Na_V1.2$ and $Na_V1.6$.[33] Interestingly, residues forming the contours of the acylsulfonamide binding pocket show high sequence homology across $Na_V$ isoforms, suggesting that selectivity for this class is likely an allosteric phenomenon. Nonetheless, the disparate binding pockets for these two inhibitor classes provide a clear rationale for their historically divergent patterns of selectivity.

Our structure of **GDC-0310** provides a structural rationale for the relative slow dissociation kinetics of acylsulfonamide inhibitors compared to arylsulfonamides.[33] Specifically, the acylsulfonamide pocket is buried more deeply into the plasma membrane than the arylsulfonamide pocket, and may be available only through a membrane-access pathway that first involves partitioning of the molecule into the intramembrane space. In comparison, the arylsulfonamide pocket is open to the outer membrane interface, offering access from the solvent compartment. Slow dissociation kinetics are known to be associated with membrane-access pathways for small molecules binding to transmembrane proteins.[32,39] For example, the long duration of action of salmeterol (a long-acting $\beta_2$ adrenergic receptor agonist) is proposed to be a result of its membrane partitioning properties. In comparison, salbutamol, which binds to the same target and site but through a solvent-access pathway, shows much faster dissociation from the receptor.[40-46]

In addition to offering valuable information for retrospective analysis of historical $Na_V1.7$ VSD4 domain inhibitors, the structure of **GDC-0310** inspired the development of a class of structurally differentiated molecules that bind to a novel conformation of the receptor. These hybrid molecules bridge both the S2/S3 and S3/S4 helical gaps, with the anionic moiety situated centrally, interacting with the arginine network at the core of the domain. We have demonstrated proof-of-concept that potent hybrid inhibitors can be designed with fewer membrane-associated elements than prior generation $Na_V1.7$ inhibitors, and anticipate that this will offer opportunities to develop molecules with improved lipophilic ligand efficiency and/or differentiated pharmacokinetic profiles. Hybrid inhibitors can also access selectivity determinants from both the S2/S3 and S3/S4 pockets simultaneously, offering a tantalizing opportunity to develop exquisite selectivity over other $Na_V$ isoforms.

Beyond the scope of $Na_V$ channel inhibitors, our experiences may also offer lessons translatable to small molecule modulators of other transmembrane proteins. Specifically, it is noteworthy to observe that both aryl- and acylsulfonamide inhibitors have access to cryptic pockets that are not observable in the co-structures of the parent proteins. Designing small molecules to “push” on a structural protein element is a

common strategy in medicinal chemistry, but it is often challenging to predict when such efforts will afford new, well-defined binding pockets. As such, these designs are often met with failure and quickly abandoned. However, some scenarios exist in which a cryptic pocket is more likely to be found. In these cases, medicinal chemists are more often emboldened to continue experimenting with designs that push into new areas of a protein binding pocket, even when met with initial failure. For example, type II kinase inhibitors can be rationally designed starting from a type I inhibitor structure by appending groups that push through the DFG into the cryptic back pocket.[47] This pocket is not visible from the type I inhibitor structure, but knowledge of the protein dynamics associated with the DFG-in/DFG-out transition provides a rationale for exploring these designs. We speculate that transmembrane intrahelical domains, particularly those in ion channels, transporters, and GPCRs, may present similarly privileged protein structural motifs that are rich with opportunities for the discovery of druggable cryptic pockets.

In summary, we have developed a robust pipeline for high-resolution structural determination of small-molecule bound $Na_V1.7$ channels suitable for use in iterative structure-based drug design campaigns. We also report the first co-structure of an acylsulfonamide inhibitor bound to the VSD4 domain of $Na_V1.7$, revealing an unexpected and unique binding mode. This finding provides clear rationale for previously unexplainable divergence in the in vitro pharmacological behavior between the two inhibitor classes, and inspired the development of hybrid inhibitors that merge structural features from both inhibitor classes, engaging the receptor in a novel conformation. Our findings highlight the power of cryoEM as an enabling drug discovery technology and offer interesting learnings regarding ion channel structural dynamics that are potentially applicable to other related targets and target classes.

## Materials and Methods

**Generation of** VSD4-$Na_V1.7$-$Na_V$Pas channel constructs

VSD4-$Na_V1.7$-$Na_V$Pas chimeric constructs were used as described previously.[21] In brief, optimized coding DNA for $Na_V1.7$ VSD4-$Na_V$PaS chimeras with N-terminal tandem StrepII and FLAG tag was cloned into a pRK vector with CMV promoter. HEK293 cells in suspension were cultured in SMM 293T-I medium under 5% $CO_2$ at 37°C and transfected using PEI when the cell density reached $4 \times 10^6$ cells per ml. Transfected cells were harvested 48 hours after transfection. The Dc1a toxin coding DNA from *Diguetia canities* was cloned into a modified pAcGP67A vector downstream of the polyhedron promoter and an N-terminal 6x HIS tag. Recombinant baculovirus was generated using the Baculogold system (BD Biosciences) and *Trichoplusia ni* cells were infected for protein production. The supernatant was harvested 48 h post-infection.

**Protein expression and purification:**

One hundred fifty grams of cell pellet was resuspended in 500mL of 25mM Hepes pH 7.5, 200mM NaCl, 1ug/mL benzonase, 1mM PMSF, and Roche protease inhibitor tablets. Cells were lysed by dounce homogenization. Proteins were solubilized by addition of 2% GDN (Avanti) with 0.3% cholesteryl hemisuccinate (Avanti) for 2 hours at 4°C. Cell debris was separated by ultracentrifugation at 40,000 rpm at 4°C. Affinity purification

401 using anti-Flag resin was performed by batch binding for 1 hour at 4°C. The resin was
402 washed with 5CV Purification Buffer (25mM Hepes pH 7.5, 200mM NaCl, 0.01%
403 GDN). Another 5CV wash was performed using Purification Buffer supplemented with
404 5mM ATP and 10mM $MgCl_2$. Proteins were eluted in 6 CV Purification Buffer with
405 300ug/mL Flag peptide. Proteins were subjected to another round of affinity purification
406 using StrepTactin resin (IBA). Proteins were eluted, and concentrated to ~ 5 mg/mL. For
407 the compound **2** containing sample, instead of nanodisc reconstitution VSD4-$Na_V$1.7-
408 $Na_V$Pas was incubated overnight with Dc1a toxin at a 2:1 molar ration of toxin:VSD4-
409 $Na_V$1.7-$Na_V$Pas. The eluted sample was concentrated to 100uL, and separated on
410 Superose 6 3.2/300.
411
412 For nanodisc reconstitution used for the samples containing **GNE-3565, GDC-0310** and
413 compound **4**, a 200-molar excess of lipid mix (3POPC:1POPE:1POPG resuspended in
414 50mM Hepes pH7.5, 100mM NaCl, 5mM $MgCl_2$, 1% CHAPS) was added to detergent-
415 solubilized protein and incubated on ice for 30 minutes. A four-molar excess of scaffold
416 protein (MSP1E3D1, Sigma) was added to the protein-lipid mix, and incubated on ice for
417 another 30 minutes. To remove detergent, BioBeads (Bio-Rad) were added to 0.25
418 mg/mL, and incubated overnight at 4°C. To remove the empty nanodiscs, the sample was
419 subjected to a round of affinity purification using Strep-Tactin (IBA). The eluted sample
420 was concentrated to 100uL, and separated on Superose 6 3.2/300. Peak fractions were
421 combined, and split into four samples. Fifty uM of the small molecule of interest was
422 added to each sample, and incubated at 22°C for 10 minutes. Samples were crosslinked
423 with 0.05% glutaraldehyde (Electron Microscopy Sciences) then quenched with 1M Tris
424 pH 7.0. Samples at 2 mg/mL were used for grid freezing.
425
426
427 **CryoEM sample preparation and data acquisition**
428 CryoEM grids for the small molecule VSD4-$Na_V$1.7-$Na_V$Pas chimeric complexes shown
429 in this study were prepared as follows: For the **GDC-0310** and compound **4** VSD4-
430 $Na_V$1.7-$Na_V$Pas complexes, holey carbon grids (Ultrafoil 25 nM Au R 0.6/1 300 mesh;
431 Quantifoil) were incubated with a thiol reactive, self-assembling reaction mixture of
432 4mM monothiolalkane(C11)PEG6-OH (11-mercaptoundecyl) hexaethyleneglycol (SPT-
433 0011P6, SensoPath Technologies, Inc., Bozeman, MT). Grids were incubated with this
434 self-assembled monolayer (SAM) solution for 24 hours and afterwards rinsed with EtOH.
435 3 µl of the sample was applied to the grid and blotted with Vitrobot Mark IV
436 (Thermofisher) using 3.5 s blotting time with 100% humidity and plunge-frozen in liquid
437 ethane cooled by liquid nitrogen. The **GNE-3565** VSD4-$Na_V$1.7-$Na_V$Pas complex was,
438 similarly as described above, applied to a holey carbon grid (Ultrafoil 25 nM Au R
439 1.2/1,3 300 mesh; Quantifoil) pretreated with SAM solution. The grid was blotted single-
440 sided with a Leica EM GP (Leica) using 3 s blotting time with 100% humidity and
441 plunge-frozen in liquid ethane cooled by liquid nitrogen. For compound **2** VSD4-$Na_V$1.7-
442 $Na_V$Pas-DC1a complex, holey carbon grids (Ultrafoil 25 nM Au R 2/2 200 mesh;
443 Quantifoil) were glow-discharged for 10 s using the Solarus plasma cleaner (Gatan). 3 µl
444 of the sample was applied to the grid and blotted with Vitrobot Mark IV (Thermofisher)
445 using 2.5 s blotting time with 100% humidity and plunge-frozen in liquid ethane cooled
446 by liquid nitrogen.

447
448 Movie stacks for compound **2** VSD4-$Na_V$1.7-$Na_V$Pas-DC1a complex were collected
449 using SerialEM[48] on a Titan Krios operated at 300 keV with bioquantum energy filter
450 equipped with a K2 Summit direct electron detector camera (Gatan). Images were
451 recorded at 165,000 × magnification corresponding to 0.824 Å per pixel, using a 20 eV
452 energy slit. Each image stack contains 50 frames recorded every 0.2 s for an accumulated
453 dose of ∼50 e Å−2 and a total exposure time of 10 s. Images were recorded with a set
454 defocus range of 0.5 to 1.5 µm.
455
456 Movie stacks for **GNE-3565, GDC-0310** and compound **4** VSD4-$Na_V$1.7-$Na_V$Pas
457 complexes were collected using SerialEM on a Titan Krios G3i (ThermoFisher Scientific,
458 Waltham, MA) operated at 300 keV with bioquantum energy filter equipped with a K3
459 Summit direct electron detector camera (Gatan Inc, Pleasanton, CA). Images were
460 recorded in EFTEM mode at 105,000 × magnification corresponding to 0.838 Å per
461 pixel, using a 20 eV energy slit. Each image stack contains 60 frames recorded every 0.05
462 s for an accumulated dose of ∼60 e Å−2 and a total exposure time of 3 s. Images were
463 recorded with a set defocus range of 0.5 to 1.5 µm.
464
465 **CryoEM data processing**
466 CryoEM data were processed using a combination of the RELION[49] and cisTEM[50]
467 software packages, similarly as described previously[51] and as illustrated in Suppl. Figure
468 2 and 3.
469
470 Movies were corrected for frame motion using the MotionCor2[52] implementation in
471 RELION and contrast-transfer function parameters were fit using the 30-4.5 Å band of
472 the spectrum with CTFFIND-4.[53] CTF fitted images were filtered on the basis of the
473 detected fit resolution better than 6-10 Å. Particles were picked by template-matching
474 with gautomatch (https://www2.mrc-lmb.cam.ac.uk/research/locally-developed-
475 software/zhang-software/#gauto) using a 30 Å low-pass filtered apo VSD4-$Na_V$1.7-
476 $Na_V$Pas reference structure. Particles were sorted during RELION 2D classification and
477 selected particles were imported into cisTEM for 3D refinements. 3D reconstructions
478 were obtained after auto-refine and manual refinements with a mask around the channel
479 (excluding the detergent micelle) and by applying low-pass filter outside the mask (filter
480 resolution 20 Å) and a score threshold of 0.10-0.30, so that only the best-scoring 10-30%
481 of particle images would be included in the 3D reconstruction at each cycle. The weight
482 outside of the mask was set to 0.8. No data beyond 3.0 Å for compound **4**, 3.4 Å for
483 **GDC-0310**, 3.7Å **GNE-3565** and 4.0 Å for compound **2** were used in the refinements.
484 Phenix ResolveCryoEM[54] density modification was applied to each of the reconstructions
485 to obtained the final map used for model building. Local resolution was determined in
486 cisTEM using a reimplementation of the blocres algorithm.
487
488 **Model building and structure analysis**
489 The previously determined VSD4-$Na_V$1.7-$Na_V$Pas model (PDB: 6NT3)[21] was fit as a
490 rigid body into the cryoEM map. After manual adjustments, multiple rounds of real space
491 refinement using the phenix.real_space_refinement tool[55] was used to correct structural
492 differences between the initial model and the map. The small molecule coordinates were

493 generated with eLBOW,[56] placed and manually adjusted in Coot,[57] energy minimized
494 with MOE (Chemical Computing Group ULC,) and refined with real space refinements
495 in Phenix[55]. The model was validated using phenix.validation_cryoem[58] with built-in
496 MolProbity scoring.[59] Figures were made using PyMOL (The PyMOL Molecular
497 Graphics System, v.2.07 Schrödinger, LLC), UCSF Chimera,[60] and UCSF ChimeraX.[61]
498
499 **Chemical synthesis**
500 The synthesis of **GNE-3565**, **GDC-0310**, and compound **1** have been previously
501 reported.[12,15,62] The synthesis and characterization of compounds **2-5** are described in the
502 supporting information.
503
504 **$Na_V$1.7 Syncropatch electrophysiology potency**
505 cDNAs for $Na_V$1.7 (NM_002977) were stably expressed in Chinese Hamster Ovary
506 (CHO) cells. Sodium currents were measured in the whole-cell configuration using
507 Syncropatch 384PE (NanIon Technologies, Germany). 1NPC®-384 chips with custom
508 medium resistance and single hole mode were used. Internal solution consisted of (in
509 mM): 110 CsCl, 10 CsCl, 20 EGTA, and 10 Hepes (pH adjusted to 7.2); and external
510 solution contains (in mM): 60 NMDG, 80 NaCl, 4 KCl, 1 $MgCl_2$, 2 $CaCl_2$, 2 D-Glucose
511 monohydrate, 10 Hepes (pH adjusted to 7.4 with NaOH).
512
513 After system flushing, testing compounds were dissolved in external solution containing
514 0.1% Pluronic F-127. 10µl cells were added to the chip from a cell hotel, and a negative
515 pressure of −50 mBar was applied to form a seal. Following treatment with seal enhancer
516 solution and wash-off with external solution, negative pressure of −250 mbar was applied
517 for 1 second to achieve the whole-cell configuration, followed by three washing steps in
518 external solution. 20µl of compounds were added to 40µl in each well (1:3 dilution of
519 compounds), and after mixing, 20µl was removed so the volume was retained at 40 ul.
520 After approximately 13 minutes recording, 20µl/well of 2 uM TTX was added to achieve
521 full block.
522
523 For voltage protocol, a holding potential of -50 mV was applied during the whole
524 experiment. A depolarizing step was applied to -10mV for 10ms, followed by a
525 hyperpolarization step to -150 mV for 20 ms to allow channel recovery from inactivation.
526 A second depolarizing step was applied from -150mV to -10mV for 10 ms, where
527 currents were measured to derive blocking effects of compounds. Inhibition was
528 determined based on 7.5 min of compound incubation.
529
530 **Figure Legends:**
531
532 **Figure 1: (A)** Schematic of the VSD4-$Na_V$1.7-$Na_V$Pas channel. The portions humanized
533 to the $Na_V$1.7 sequence are shown in green. N-terminal domain (NTD) and CTD are
534 indicated. **(B)** Side view of the single-particle cryo-EM reconstruction of VSD4- $Na_V$1.7-
535 $Na_V$Pas channel **(C-D)** Cartoon representations of the Top and Side views of VSD4-
536 $Na_V$1.7-$Na_V$Pas channel. Individual VSD domains are indicated. VSD4 is highlighted in
537 green. **(E)** Localization of water molecules (in red) in the VSD4-$Na_V$1.7-$Na_V$Pas channel
538 structure. VSD4 is highlighted in green.

**Figure 2: (A)** Chemical structures of arylsulfonamide **GNE-3565**. **(B,C)** Top and Side views of VSD4-$Na_V$1.7-$Na_V$Pas channel bound to **GNE-3565**. VSD4 is highlighted in green, **GNE-3565** in magenta. **(D)** Extracellular view of VSD4-$Na_V$1.7-$Na_V$Pas arylsulfonamide receptor site is shown with select side chains rendered as sticks. **(E)** The cryoEM map surrounding the ligand **GNE-3565** is shown in mesh representation. **(F)** View towards the membrane highlighting key interactions with the **GNE-3565** warhead. **(G)** View from the membrane highlighting key interactions with the **GNE-3565** central phenyl ring.

**Figure 3: (A)** Chemical structures of acylsulfonamide **GDC-0310**. **(B)** Top and Side views of VSD4-$Na_V$1.7-$Na_V$Pas channel bound to **GDC-0310**. VSD4 is highlighted in green, **GDC-0310** in magenta. **(D)** Extracellular view of VSD4-$Na_V$1.7-$Na_V$Pas acylsulfonamide receptor site is shown with select side chains rendered as sticks. **(E)** The cryoEM map surrounding the ligand **GDC-0310** is shown in mesh representation. **(F)** View towards the membrane highlighting key interactions with the **GDC-0310** warhead. **(G)** View from the membrane highlighting van der Waals interactions with the **GDC-0310** cyclopropyl substituent. The alpha-methylbenzylamine tail region sits almost entirely within the lipid bilayer.

**Figure 4: (A)** Illustration of hybrid molecule design approach. **(B)** Arylsulfonamide, acylsulfonamide and hybrid molecule poses **(C)** Hybridization strategy and molecule optimization. Highlighted are molecule **2** and molecule **4** **(D)** Extracellular view of VSD4-$Na_V$1.7-$Na_V$Pas bound to the hybrid molecule **2**. **(E)** View towards the membrane highlighting key interactions with the anionic group. **(F)** View from the membrane highlighting the lack of a stacking interaction between Y1537 and the phenyl ring. **(G)** Extracellular view of VSD4-$Na_V$1.7-$Na_V$Pas bound to the hybrid molecule **4**. **(H)** View towards the membrane highlighting key interactions with the anionic group. **(I)** View from the membrane highlighting the π-stacking interaction between Y1537 and the phenyl ring.

**Acknowledgments**

We are grateful to BMR and RMG for construct generation and protein scale-up. We are thankful to Cameron Noland for help with the biochemistry of the VSD4-$Na_V$1.7-$Na_V$Pas channel system. We thank Tommy Lai and Wenfeng Liu for chemistry support.

**Material and Data Availability:** All data generated or analyzed during this study are included in the manuscript and supporting files. The $Na_V$1.7-$Na_V$Pas/GNE-3565 coordinates and cryo-EM maps were deposited in the PDB: XXX and EMDB: EMD-XXX, respectively. The $Na_V$1.7-$Na_V$Pas/GDC-0310 coordinates and cryo-EM maps were deposited in the PDB: XXX and EMDB: EMD-XXX, respectively. The $Na_V$1.7-$Na_V$Pas bound to the hybrid molecule **2** coordinates and cryo-EM maps were deposited in the PDB: XXX and EMDB: EMD-XXX, respectively. The $Na_V$1.7-$Na_V$Pas bound to the

hybrid molecule **4** coordinates and cryo-EM maps were deposited in the PDB: XXX and EMDB: EMD-XXX, respectively. Requests for materials should be addressed to J.C.T.

## References


1. W. A. Catterall, A. L. Goldin, S. G. Waxman, International Union of Pharmacology. XLVII. Nomenclature and structure-function relationships of voltage-gated sodium channels. *Pharmacol. Rev.* **57**, 397 (2005).
2. C. A. Ahern, J. Payandeh, F. Bosmans, B. Chanda, The hitchhiker's guide to the voltage-gated sodium channel galaxy. *J. Gen. Physiol.* **147**, 1 (2016).
3. S. D. Dib-Hajj, Y. Yang, J. A. Black, S. G. Waxman, The Na(V)1.7 sodium channel: from molecule to man. *Nat. Rev. Neurosci.* **14**, 49 (2013).
4. J. Payandeh, D. H. Hackos, Selective ligands and drug discovery targeting the voltage-gated sodium channel $Na_v1.7$. *Handb. Exp. Pharmacol.* **246**, 271 (2018).
5. S. J. McKerrall, D. P. Sutherlin, $Na_v1.7$ inhibitors for the treatment of chronic pain. *Bioorg. Med. Chem. Lett.* **28**, 3141 (2018).
6. M. de Lera Ruiz, R. L. Kraus, Voltage-gated sodium channels: structure, function, pharmacology, and clinical indications. *J. Med. Chem.* **58**, 7093 (2015).
7. K. McCormack, *et al.*, Voltage sensor interaction site for selective small molecule inhibitors of voltage-gated sodium channels. *Proc. Natl. Acad. Sci. USA* **110**, E2724 (2013).
8. N. A. Swain, *et al.,* Discovery of clinical candidate 4-[2-(5-amino-1H-pyrazol-4-yl)-4-chlorophenoxy]-5-chloro-2-fluoro-N-1,3-thiazol-4-ylbenzenesulfonamide (PF-05089771): design and optimization of diaryl ether aryl sulfonamides as selective inhibitors of $Na_V1.7$. *J. Med. Chem.* **60**, 7029 (2017).
9. A. McDonnell, *et al.,* Efficacy of the $Na_V1.7$ blocker PF-05089771 in a randomised, placebo-controlled, double-blind clinical study in subjects with painful diabetic peripheral neuropathy. *Pain* **159**, 1465 (2018).
10. P. Siebenga, *et al.*, Lack of detection of the analgesic properties of PF-05089771, a selective $Na_V1.7$ inhibitor, using a battery of pain models in healthy subjects. *Clin. Transl. Sci.* **13**, 318 (2020).
11. M. E. Rothenberg, *et al.*, Safety, tolerability, and pharmacokinetics of GDC-0276, a novel $Na_V1.7$ inhibitor, in a first-in-human, single- and multiple-dose study in healthy volunteers. *Clin. Drug Investig.* **39**, 873 (2019).
12. B. S. Safina, *et al.*, Discovery of acyl-sulfonamide $Na_V1.7$ inhibitors GDC-0276 and GDC-0310. *J. Med. Chem.* **64**, 2953 (2021).
13. S. Noreng, T. Li, J. Payandeh, Structural pharmacology of voltage-gated sodium channels. *J. Mol. Bio.* **433**, 166967 (2021).
14. S. Ahuja, *et al.*, Structural basis of Nav1.7 inhibition by an isoform-selective small-molecule antagonist. *Science* **350**, aac5464 (2015).
15. S. Sun, *et al.*, Identification of selective acyl sulfonamide-cycloalkylether inhibitors of the voltage-gated sodium channel ($Na_V$)1.7 with potent analgesic activity. *J. Med. Chem.* **62**, 908 (2019).
16. M. Congreve, J. M. Dias, F. H. Marshall, Structure-based drug design for G protein-coupled receptors. *Prog. Med. Chem.* **53**, 1 (2014).

17. Y. Cheng, Membrane protein structural biology in the era of single particle cryo-EM. *Curr. Opin. Struct. Biol.* **52**, 58 (2018).
18. A. Balestrini, *et al.*, A TRPA1 inhibitor suppresses neurogenic inflammation and airway contraction for asthma treatment. *J. Exp. Med.* **218**, e20201637 (2021).
19. L. Rougé, *et al.*, Structure of CD20 in complex with the therapeutic monoclonal antibody rituximab. *Science* **367**, 1224 (2020).
20. H. Xu, *et al.*, Structural basis of $Na_V1.7$ inhibition by a gating-modifier spider toxin. *Cell* **176**, 702 (2019).
21. T. Clairfeuille, et al., Structural basis of α-scorpion toxin action on $Na_V$ channels. *Science* **363**, eaav8537 (2019).
22. H. Shen, D. Liu, K. Wu, J. Lei, N. Yan, Structures of human $Na_V$ 1.7 channel in complex with auxiliary subunits and animal toxins. *Science* **363**, 1303 (2019).
23. G. Huang, *et al.*, High-resolution structures of human $Na_V1.7$ reveal gating modulation through α-π helical transition of $S6_{IV}$. *Cell Rep.* **39**, 110735 (2022).
24. H. Shen, *et al.*, Structure of a eukaryotic voltage-gated sodium channel at near-atomic resolution. *Science* **355**, eaal4326 (2017).
25. H. Shen, *et al.*, Structural basis for the modulation of voltage-gated sodium channels by animal toxins. *Science* **362**, eaau2596 (2018).
26. M. Weiss, *et al.*, Sulfonamides as selective $Na_V1.7$ inhibitors: optimizing potency and pharmacokinetics while mitigating metabolic liabilities, *J. Med. Chem.* **60**, 5969 (2017).
27. R. F. Graceffa, *et al.*, Sulfonamides as selective $Na_V1.7$ inhibitors: optimizing potency, pharmacokinetics, and metabolic properties to obtain atropisomeric quinolinone (AM-0466) that affords robust in vivo activity, *J. Med. Chem.* **60**, 5990 (2017).
28. S. J. McKerrall, *et al.*, Structure- and ligand-based discovery of chromane arylsulfonamide $Na_V1.7$ inhibitors for the treatment of chronic pain, *J. Med. Chem.* **62**, 4091 (2019).
29. A. J. Roecker, *et al.*, Discovery of arylsulfonamide $Na_V1.7$ inhibitors: IVIVC, MPO methods, and optimization of selectivity profile, *ACS Med. Chem. Lett.* **12**, 1038 (2021).
30. T. Focken, *et al.*, Discovery of aryl sulfonamides as isoform-selective inhibitors of $Na_V1.7$ with efficacy in rodent pain models, *ACS Med. Chem. Lett.* **7**, 277 (2016)
31. Y-J. W., *et al.*, Development of new benzenesulfonamides as potent and selective $Na_V1.7$ inhibitors for the treatment of pain, *J. Med. Chem.* **60**, 2513 (2017).
32. J. Payandeh, M. Volgraf, Ligand binding at the protein-lipid interface: strategic considerations for drug design. *Nat. Rev. Drug Discov.* **20**, 710 (2021).
33. G. Bankar, et al., Selective $Na_V1.7$ antagonists with long residence time show improved efficacy against inflammatory and neuropathic pain. *Cell Rep.* **24**, 3133 (2018).
34. G. Luo, *et al.*, Discovery of indole- and indazole-acylsulfonamides as potent and selective $Na_V1.7$ inhibitors for the treatment of pain, *J. Med. Chem.* **62**, 831 (2019).

35. E. F. DiMauro, *et al.*, Application of a parallel synthetic strategy in the discovery of biaryl acyl sulfonamides as efficient and selective $Na_V1.7$ inhibitors, *J. Med. Chem.* **59**, 7818 (2016).
36. T. Focken, *et al.*, Design of conformationally constrained acyl sulfonamide isosteres: identification of N-([1,2,4]triazolo[4,3-a]pyridin-3-yl)methane-sulfonamides as potent and selective $hNa_V1.7$ inhibitors for the treatment of pain, *J. Med. Chem.* **61**, 4810 (2018).
37. X. Li, et al., Structural basis for modulation of human $Na_V1.3$ by clinical drug and selective antagonist. *Nat. Commun.* **13**, 1286 (2022).
38. N. K. Kotla, K. A. Kumari, S. K. Gunda, M. Shaik, 3D-QSAR and molecular docking studies of acylsulfonamides as $Na_V1.7$ inhibitors in chronic pain. *Res. J. Life Sci. Bioinform. Pharm. Chem. Sci.* **5**, 120 (2019).
39. R. P. Mason, D. G. Rhodes, L. G. Herbette, Reevaluating equilibrium and kinetic binding parameters for lipophilic drugs based on a structural model for drug interactions with biological membranes. *J. Med. Chem.* **34**, 869 (1991).
40. R. A. Coleman, M. Johnson, A. T. Nials, C. J. Vardey, Exosites: their current status, and their relevance to the duration of action of long- acting beta 2-adrenoceptor agonists. *Trends Pharmacol. Sci.* **17**, 324 (1996).
41. G. P. Anderson, A. Lindén, K. F. Rabe, Why are long-acting beta-adrenoceptor agonists long-acting? *Eur. Respir. J.* **7**, 569 (1994).
42. M. Masureel, *et al.*, Structural insights into binding specificity, efficacy and bias of a β2 AR partial agonist. *Nat. Chem. Biol.* **14**, 1059 (2018).
43. R. P. Austin, *et al*., QSAR and the rational design of long- acting dual D2-receptor/beta 2-adrenoceptor agonists. *J. Med. Chem*. **46**, 3210 (2003).
44. D. G. Rhodes, R. Newton, R. Butler, L. Herbette, Equilibrium and kinetic studies of the interactions of salmeterol with membrane bilayers. *Mol. Pharmacol.* **42**, 596 (1992).
45. D. A. Sykes, *et al.*, Observed drug- receptor association rates are governed by membrane affinity: the importance of establishing "micro- pharmacokinetic/ pharmacodynamic relationships" at the β2-adrenoceptor. *Mol. Pharmacol.* **85**, 608 (2014).
46. C. J. Dickson, *et al.*, Uncoupling the structure−activity relationships of β2 adrenergic receptor ligands from membrane binding. *J. Med. Chem.* **59**, 5780 (2016).
47. Z. Zhao, *et al.*, Exploration of type II binding mode: a privileged approach for kinase inhibitor focused drug discovery? *ACS Chem. Biol.* **9**, 1230 (2014).
48. D. N. Mastronarde, Automated electron microscope tomography using robust prediction of specimen movements. *J. Struct. Biol.* **152**, 36 (2005).
49. S. H. W. Scheres, RELION: implementation of a Bayesian approach to cryo-EM structure determination. *J. Struct. Biol.* **180**, 519 (2012).
50. T. Grant, A. Rohou, N. Grigorieff, *cis*TEM, user-friendly software for single-particle image processing. *Elife* **7**, e35383 (2018).
51. M. Kschonsak, *et al.* Structural architecture of the human NALCN channelosome. *Nature* **603**, 180 (2022).
52. S. Q. Zheng *et al.* MotionCor2: anisotropic correction of beam-induced motion for improved cryo-electron microscopy. *Nature Methods* **14**, 331 (2017).

53. A. Rohou, N. Grigorieff, CTFFIND4: Fast and accurate defocus estimation from electron micrographs. *J. Struct. Biol.* **192**, 216 (2015).
54. T. C. Terwilliger, S. J. Ludtke, R. J. Read, P. D. Adams, P. V. Afonine, Improvement of cryo-EM maps by density modification. *Nature Methods* **17**, 923 (2020).
55. P. V. Afonine, *et al*. Real-space refinement in PHENIX for cryo-EM and crystallography. *Acta Crystallogr. D. Struct. Biol.* **74**, 531 (2018).
56. N. W. Moriarty, R. W. Grosse-Kunstleve, P. D. Adams, electronic Ligand Builder and Optimization Workbench (eLBOW): a tool for ligand coordinate and restraint generation. *Acta Crystallogr. D. Biol. Crystallogr.* **65**, 1074 (2009).
57. P. Emsley, B. Lohkamp, W. G. Scott, K. Cowtan, Features and development of Coot. *Acta Crystallogr. D. Biol. Crystallogr.* **66**, 486 (2010).
58. P. V. Afonine, *et al*. New tools for the analysis and validation of cryo-EM maps and atomic models. *Acta Crystallogr. D Struct. Biol.* **74**, 814 (2018).
59. C. J. Williams, *et al*. MolProbity: More and better reference data for improved all-atom structure validation. *Protein Sci.* **27**, 293 (2018).
60. E. F. Pettersen, *et al*. UCSF Chimera--a visualization system for exploratory research and analysis. *J. Comput. Chem.* **25**, 1605 (2004).
61. T. D. Goddard, *et al.* UCSF ChimeraX: Meeting modern challenges in visualization and analysis. *Protein Sci.* **27**, 14 (2018).
62. D. Sutherlin *et al.* Therapeutic compounds and methods of use thereof. US11028075B2, June 8, 2021.

**Supporting Information**

# CryoEM reveals unprecedented binding site for $Na_V1.7$ inhibitors enabling rational design of potent hybrid inhibitors

Marc Kschonsak[1*], Christine C. Jao[1*], Christopher P. Arthur[1], Alexis L. Rohou[1], Philippe Bergeron[2], Daniel Ortwine[2], Steven J. McKerrall[2], David H. Hackos[3], Lunbin Deng[3], Jun Chen[4], Peter S. Dragovich[2], Matthew Volgraf[2], Matthew R. Wright[5], Jian Payandeh[1,#], Claudio Ciferri[1,#], John C. Tellis[2,#]

[1]Genentech Inc., Structural Biology; South San Francisco, CA, United States.
[2]Genentech Inc., Discovery Chemistry; South San Francisco, CA, United States.
[3]Genentech Inc., Neuroscience; South San Francisco, CA, United States.
[4]Genentech Inc., Biochemical and Cellular Pharmacology; South San Francisco, CA, United States.
[5]Genentech Inc., Drug Metabolism and Pharmacokinetics; South San Francisco, CA, United States.

[#]Corresponding authors. Email: jpayandeh@exelixis.com (J.P); ciferri.claudio@gene.com (C.C.); tellis.john@gene.com (J.C.T.).

41 **Table S1. Cryo-EM data collection, refinement and validation statistics.**

42

| | **GNE-3565** VSD4-$Na_V1.7$-$Na_VPas$ complex | **GDC-0310** VSD4-$Na_V1.7$-$Na_VPas$ complex | **GNE-1305** VSD4-$Na_V1.7$-$Na_VPas$ complex | **GNE-9296** VSD4-$Na_V1.7$-$Na_VPas$-DC1a complex |
|---|---|---|---|---|
| **Data Collection** | | | | |
| Magnification | 105,000x | 105,000x | 165,000x | 165,000x |
| Voltage (kV) | 300 | 300 | 300 | 300 |
| Electron exposure (e/Å$^2$) | 64 | 64 | 64 | 48 |
| Defocus range (μm) | 0.5-1.5 | 0.5-1.5 | 0.5-1.5 | 0.5-1.5 |
| Pixel size (Å) | 0.838 | 0.838 | 0.838 | 0.824 |
| Symmetry imposed | C1 | C1 | C1 | C1 |
| Initial particle images | 3,686,837 | 2,253.983 | 2,741,402 | 1,774,062 |
| Final particle images | 964,572 | 795,792 | 1,201,168 | 826,525 |
| Map resolution (Å) overall | 2.9 | 2.5 | 2.2 | 3.1 |
| FSC threshold | 0.143 | 0.143 | 0.143 | 0.143 |
| Map resolution range (Å) | 2.7-33.5 | 2.3-33.5 | 2.1-33.5 | 3.3-33.0 |
| **Refinement** | | | | |
| Initial models used (PDB code) | 6NT3 | 6NT3 | 6NT3 | 6NT3 |
| Model resolution (Å) | 2.9 | 1.9 | 1.7 | 2.5 |
| FSC threshold | 0.5 | 0.5 | 0.5 | 0.5 |
| Model composition | | | | |
| Non-hydrogen atoms | 9396 | 9557 | 9616 | 9734 |
| Protein residues | 1115 | 1115 | 1117 | 1159 |
| Waters | 0 | 78 | 111 | 0 |
| Ligands | 13 | 13 | 14 | 13 |
| B factors (Å$^2$) | | | | |
| Protein | 25.62 | 12.42 | 6.27 | 24.05 |
| Ligand | 35.81 | 15.79 | 10.33 | 40.62 |
| Water | N/A | 8.11 | 6.54 | N/A |
| R.m.s. deviations | | | | |
| Bond lengths (Å) | 0.004 | 0.005 | 0.005 | 0.005 |
| Bond angles (°) | 0.931 | 1.018 | 0.994 | 0.941 |
| Validation | | | | |
| MolProbity score | 1.30 | 1.19 | 1.14 | 1.38 |
| Clashscore | 5.47 | 4.09 | 3.51 | 6.42 |
| Poor rotamers (%) | 0.10 | 0.20 | 0.61 | 0.00 |
| Ramachandran Plot | | | | |
| Favored (%) | 98.45 | 98.27 | 98.19 | 97.90 |
| Allowed (%) | 1.55 | 1.73 | 1.81 | 2.10 |
| Disallowed (%) | 0.00 | 0.00 | 0.00 | 0.00 |
| | | | | |

43

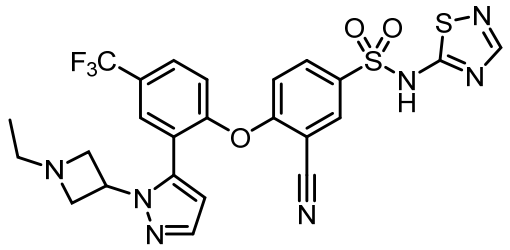


**GX-936**

**Supplementary Figure 1:** Structure of arylsulfonamide inhibitor **GX-936**

## Chemical compound synthesis and characterization

### General Considerations

All commercial solvents and reagents were used without additional purification unless indicated otherwise. $^{1}$H NMR spectra were measured on Bruker Avance III 300, 400, or 500 MHz spectrometers. Chemical shifts (in ppm) were referenced to tetramethylsilane as an internal standard (δ = 0 ppm). Reaction progress was monitored by either a Shimadzu LCMS/UV system with an LC-30 AD solvent pump, Sil-30 AC autosampler, 2020 MS, SPDM30A UV detector, and CTO-20A column oven, using 2−98% acetonitrile/0.1% formic acid (or 0.01% ammonia) over 2.5 min or a Waters Acquity LCMS system using 2−98% acetonitrile/0.1% formic acid (or 0.1% ammonia) over 2 min. Flash column chromatography purifications were performed using a Teledyne Isco Combiflash Rf and Silicycle HP columns. Reverse-phase purification was done on a Phenomenex Gemini-NX C18 (30 × 100 mm, 5 µm) with a gradient of 5−95% acetonitrile/water (with 0.1% NH4OH or 0.1% formic acid) at 60 mL/min over 10 min. Preparative SFC separations were carried out on a PIC Solutions instrument, with conditions specified in the Experimental Section. High-resolution mass spectrometry (HRMS) of final compounds was obtained on a Thermo UHPLC/ QE with a Thermo-Q Exactive mass spectrometry detector using ESI ionization, following elution on an Acquity BEH C18 stationary phase (2.1 mm × 50 mm; 1.7 µm particle size) using a gradient of water/ acetonitrile (3−97% over 7 min with 0.1% formic acid in both phases). Unless stated otherwise, analytical purity was >95% as determined by LCMS using UV 254 nm detection

### Compound 2

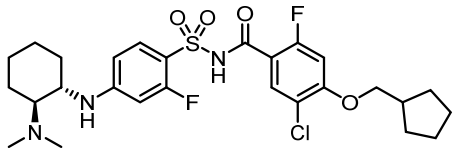


**5-chloro-4-(cyclopentylmethoxy)-*N*-((4-(((1*S*,2*S*)-2-(dimethylamino)cyclohexyl)amino)-2-fluorophenyl)sulfonyl)-2-fluorobenzamide**

**Step 1:**

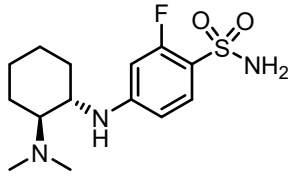


**4-(((1*S*,2*S*)-2-(dimethylamino)cyclohexyl)amino)-2-fluorobenzenesulfonamide**

A solution of (1*S*,2*S*)-$N^1$,$N^1$-dimethylcyclohexane-1,2-diamine (162 mg, 1.1 mmol), 2,4-difluorobenzenesulfonamide (200 mg, 1.0 mmol) and DIPEA (0.3 mL, 1.7 mmol) in DMSO (3 mL) was stirred at

80 °C for 16 h. After cooling to room temperature, the reaction was diluted with EtOAc (100 mL), and washed with brine (50 mL x 5). The organic lawyer was dried over anhydrous $Na_2SO_4$, filtered and concentrated in vacuo. The crude residue was purified by silica gel chromatography (solvent gradient: 0 - 10% EtOAc in petroleum ether) to afford the title compound (60 mg, 0.19 mmol) as yellow oil.
LCMS (ESI) m/z: 316.1 $[M+H]^+$.

**Step 2:**

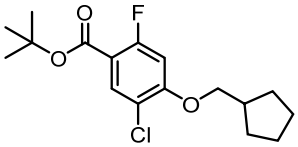

**tert-butyl 5-chloro-4-(cyclopentylmethoxy)-2-fluorobenzoate**

A mixture of tert-butyl 5-chloro-2,4-difluorobenzoate (548 g, 2.20 mol), cyclopentylmethanol (200 g, 2.00 mol) and $Cs_2CO_3$ (1.31 kg, 4.00 mol) in DMSO (3.28 L) was stirred at 80 °C for 5 hrs. The mixture was filtered and filtrate was diluted with EtOAc (3.00 L), washed with water (3.00 L x 3) and brine (1000 mL). The resultant organic layer was dried over $Na_2SO_4$, filtered, concentrated in vacuo. The residue was purified by column chromatography ($SiO_2$, Petroleum ether/Ethyl acetate = 100/1 to 50/1). The title compound (0.50 kg, crude) was obtained as light yellow oil.

**Step 3:**

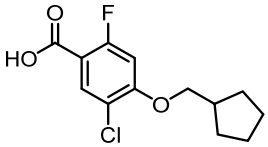

**5-chloro-4-(cyclopentylmethoxy)-2-fluorobenzoic acid**

To a solution of *tert*-butyl 5-chloro-4-(cyclopentylmethoxy)-2-fluorobenzoate (327 g, 994 mmol) in DCM (654 mL) was added TFA (654 mL) at 25 °C. The mixture was stirred at 25 °C for 24 hrs. The reaction mixture was filtered and concentrated under reduced pressure to give a residue that was triturated with 1/1 MTBE/Petroleum ether at 25 °C for 30 mins. The title compound was obtained by filtration as a white solid (83.7 g, 30.5% yield).
$^1$H NMR (400 MHz, $CDCl_3$) $\delta$ 8.04 (d, $J$ = 7.6 Hz, 1H), 6.70 (d, $J$ = 12.4 Hz, 1H), 3.96 (d, $J$ = 6.8 Hz, 2H), 2.42-2.50 (m 1H), 1.86-1.93 (m, 2H), 1.75-1.58 (m, 4H), 1.48-1.35 (m, 2H).

**Step 4:**

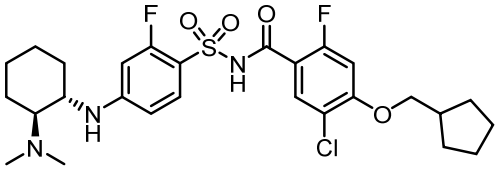

**5-chloro-4-(cyclopentylmethoxy)-*N*-((4-(((1*S*,2*S*)-2-(dimethylamino)cyclohexyl)amino)-2-fluorophenyl)sulfonyl)-2-fluorobenzamide**

To a solution of 4-(((1*S*,2*S*)-2-(dimethylamino)cyclohexyl)amino)-2-fluorobenzenesulfonamide (80 mg, 0.24 mmol) and DMAP (59 mg, 0.48 mmol) in DCM (2 mL) was added EDCI (51 mg, 0.26 mmol) and 5-chloro-4-(cyclopentylmethoxy)-2-fluoro-benzoic acid (72 mg, 0.26 mmol). The reaction was stirred at room temperature for 2 h. The reaction was quenched with 10% aqueous citric acid (5 mL). The reaction was diluted with water (10 mL) and extracted with DCM (10 mL x 3). The combined organic layers were dried over anhydrous $Na_2SO_4$, filtered and concentrated in vacuo. The crude residue was purified by silica gel chromatography (solvent gradient: 0 - 5% MeOH in DCM) to afford the title compound (40 mg, 28%) as a white solid.

$^1$H NMR (400 MHz, DMSO-$d_6$) δ 7.75 (d, $J$ = 7.6 Hz, 1H), 7.55 - 7.48 (m, 1H), 6.94 (d, $J$ = 12.4 Hz, 1H), 6.50 (s, 1H), 6.47 (s, 1H), 6.07 (d, $J$ = 10.0 Hz, 1H), 3.94 (d, $J$ = 6.8 Hz, 2H), 3.79 - 3.64 (m, 1H), 3.15 - 3.05 (m, 1H), 2.66 (s, 6H), 2.35 - 2.25 (m, 1H), 2.09 - 1.94 (m, 2H), 1.84 - 1.69 (m, 3H), 1.63 - 1.14 (m, 11H).
HRMS *m/z* calcd for $C_{27}H_{34}ClF_2N_3O_4S$ $[M+H]^+$: 570.1999. Found 570.2003.

**Compound 3**

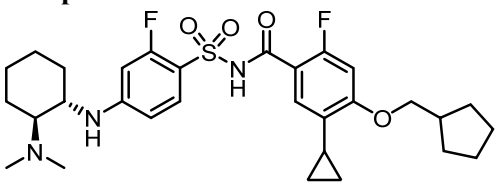

**4-(cyclopentylmethoxy)-5-cyclopropyl-N-((4-(((1S,2S)-2-(dimethylamino)cyclohexyl)amino)-2-fluorophenyl)sulfonyl)-2-fluorobenzamide**

Following the procedure described in compound **3** and replacing 5-chloro-4-(cyclopentylmethoxy)-2-fluorobenzoic acid with 4-(cyclopentylmethoxy)-5-cyclopropyl-2-fluorobenzoic acid, the title compound was obtained as a white solid.
$^1$H NMR (400 MHz, DMSO-$d_6$) δ 7.50 (t, $J$ = 8.8 Hz, 1H), 7.20 (d, $J$ = 8.8 Hz, 1H), 6.65 (d, $J$ = 12.0 Hz, 1H), 6.52 - 6.34 (m, 2H), 5.99 (s, 1H), 3.87 (d, $J$ = 6.8 Hz, 2H), 3.72 - 3.52 (m, 1H), 3.05 - 2.81 (m, 1H), 2.61 - 2.52 (m, 6H), 2.37 - 2.26 (m, 1H), 2.07 - 1.90 (m, 3H), 1.87 - 1.71 (m, 3H), 1.66 - 1.52 (m, 5H), 1.45 - 1.30 (m, 4H), 1.29 - 1.20 (m, 1H), 1.15 - 1.05 (m, 1H), 0.91 - 0.80 (m, 2H), 0.60 - 0.45 (m, 2H).
HRMS *m/z* calcd for $C_{30}H_{39}F_2N_3O_4S$ $[M+H]^+$: 576.2702. Found 576.2713.

**Compound 4**

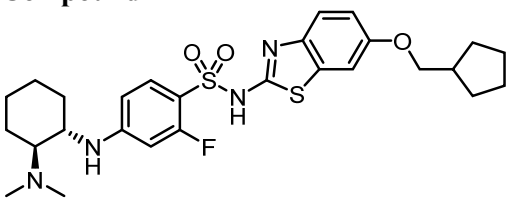

**N-(6-(cyclopentylmethoxy)benzo[d]thiazol-2-yl)-4-(((1S,2S)-2-(dimethylamino)cyclohexyl)amino)-2-fluorobenzenesulfonamide**

**Step 1:**

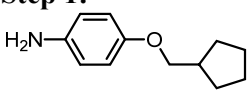

**4-(cyclopentylmethoxy)aniline**

To a stirred solution of NaH (1.32 g, 54.98 mmol, 60% in mineral oil) in DMF (20 mL) was added 4-aminophenol (2 g, 18.33 mmol) at 0 °C under nitrogen atmosphere. After stirring at 0 °C for 10 min, (bromomethyl)cyclopentane (4.48 g, 27.49 mmol) was added at 0 °C. The reaction was stirred at room temperature for 16 h. The reaction was quenched with water (100 mL) and extracted with EtOAc (100 mL x 3). The combined organic lawyers were washed with brine (100 mL), dried over anhydrous $Na_2SO_4$, filtered and concentrated in vacuo. The crude residue was purified by silica gel chromatography (solvent gradient: 10 - 20% EtOAc in petroleum ether) to afford the title compound (1.35 g, 39%) as black oil.
$^1$H NMR (400 MHz, $CDCl_3$) δ 6.77 - 6.74 (m, 2H), 6.66 - 6.63 (m, 2H), 3.76 (d, $J$ = 7.2 Hz, 2H), 3.42 (s, 2H), 2.38 - 2.27 (m, 1H), 1.86 - 1.78 (m, 2H), 1.64 - 1.58 (m, 4H), 1.39 - 1.30 (m, 2H).
LCMS (ESI) m/z: 192.2 $[M+H]^+$.

**Step 2:**

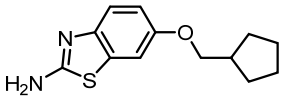

**6-(cyclopentylmethoxy)benzo[*d*]thiazol-2-amine**

The solution of 4-(cyclopentylmethoxy)aniline (1.30 g, 7.06 mmol) and potassium thiocyanate (685 mg, 7.06 mmol) in acetic acid (7.5 mL) was stirred at 0 °C for 20 min. Bromine (0.36 mL, 7.06 mmol) in acetic acid (3.5 mL) was added slowly and keep the temperature below 10 °C. Then, the mixture was stirred at room temperature for 18 h. The reaction was filtered and the filter cake was washed with acetic acid (5 mL). The filtrate was concentrated in vacuo and the crude reside was diluted with hot water (5 mL) and basified to pH>11 with $NH_3 \bullet H_2O$. The resulting precipitate was filtered and the filter cake was washed with water (5 mL). The filter cake was diluted with DCM (20 mL), dried over anhydrous $Na_2SO_4$, filtered and concentrated in vacuo. The crude residue was purified by silica gel chromatography (solvent gradient: 0 - 14% EtOAc in petroleum ether) to afford the title compound (800 mg, 46%) as a gray solid.

$^1$H NMR (400 MHz, $CDCl_3$) δ 7.43 (d, $J$ = 8.8 Hz, 1H), 7.13 (d, $J$ = 6.0 Hz, 1H), 6.93 - 6.90 (m, 1H), 5.22 (s, 2H), 3.84 (d, $J$ = 7.2 Hz, 2H), 2.41 - 2.33 (m, 1H), 1.89 - 1.81 (m, 2H), 1.68 - 1.58 (m, 4H), 1.41 - 1.33 (m, 2H).

LCMS (ESI) m/z: 249.0 $[M+H]^+$.

**Step 3:**

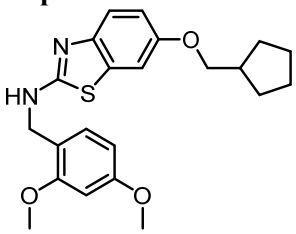

**6-(cyclopentylmethoxy)-N-(2,4-dimethoxybenzyl)benzo[d]thiazol-2-amine**

To a stirred solution of 6-(cyclopentylmethoxy)benzo[d]thiazol-2-amine (0.71 g, 2.65 mmol) and 2,4-dimethoxybenzaldehyde (0.4 g, 2.41 mmol) in DCM (12 mL) was added $TiCl(O\textit{i}\text{-}Pr)_3$ (1.86 mL, 5.54 mmol) in one portion under nitrogen atmosphere. The solution was stirred for 10 min before the portion wise addition of $NaBH(OAc)_3$ (1.53 g, 7.22 mmol) at 0 °C. The reaction was stirred at room temperature for 16 h. The reaction was quenched with saturated aqueous $NaHCO_3$ solution (50 mL), extracted with DCM (50 mL x 3). The combined organic lawyers were washed with brine (50 mL), dried over anhydrous $Na_2SO_4$, filtered and concentrated in vacuo. The crude residue was purified by silica gel chromatography (solvent gradient: 0 - 25% EtOAc in petroleum ether) to afford the title compound (0.53 g, 53%) as a white solid.

**Step 4:**

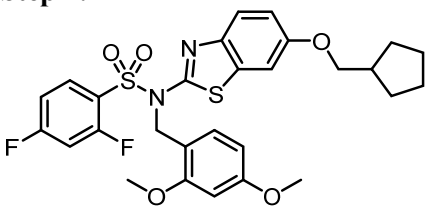

**N-(6-(cyclopentylmethoxy)benzo[d]thiazol-2-yl)-N-(2,4-dimethoxybenzyl)-2,4-difluorobenzenesulfonamide**

To a solution of 6-(cyclopentylmethoxy)-N-(2,4-dimethoxybenzyl)benzo[d]thiazol-2-amine (170 mg, 0.52 mmol) in THF (2 mL) was added LiHMDS (0.62 mL, 0.62 mmol, 1 M) at -78 °C. The reaction was stirred for 30 min at 0 °C and a solution of 2,4-difluorobenzenesulfonylchloride (0.22 g, 1.03 mmol) in THF (2 mL) was added dropwise at -78 °C. After the addition was complete, the cooling bath was removed. The reaction mixture was stirred at room temperature for 3 h. The reaction was diluted with water (30 mL) and extracted with EtOAc (50 mL x 3). The combined organic lawyers were washed with brine (50 mL), dried over anhydrous $Na_2SO_4$, filtered and concentrated in vacuo. The crude residue was purified by silica gel chromatography (solvent gradient: 0 - 30% EtOAc in petroleum ether) to afford the title compound (160 mg, 52%) as a white solid.

**Step 5:**

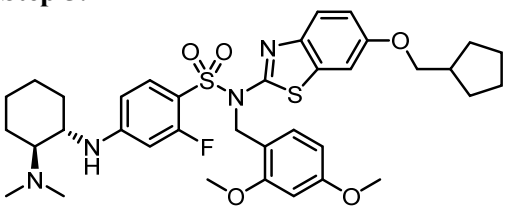

**N-(6-(cyclopentylmethoxy)benzo[d]thiazol-2-yl)-N-(2,4-dimethoxybenzyl)-4-(((1S,2S)-2-(dimethylamino)cyclohexyl)amino)-2-fluorobenzenesulfonamide**

To a solution of *N*-(6-bromothiazolo[4,5-*b*]pyridin-2-yl)-4-(((1*S*,2*S*)-2-(dimethylamino)cyclohexyl)amino)-2-fluorobenzenesulfonamide (40 mg, 0.07 mmol) in DMSO (1 mL) was added DIPEA (14 mg, 0.11 mmol) and (1*S*,2*S*)-$N_1$,$N_1$-dimethylcyclohexane-1,2-diamine (15 mg, 0.11 mmol) at room temperature. The reaction mixture was stirred at room temperature for 20 h. The reaction was quenched with saturated aqueous $NH_4Cl$ (20 mL), extracted with EtOAc (30 mL x 3). The combined organic layers were washed with brine (30 mL), dried over anhydrous $Na_2SO_4$, filtered and concentrated in vacuo to afford the title compound (48 mg, crude) as yellow oil that required no further purification.

**Step 6:**

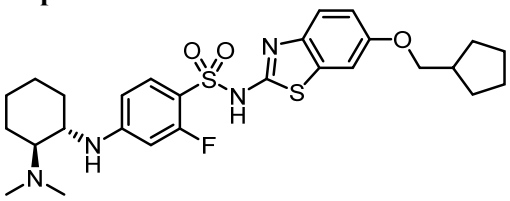

**N-(6-(cyclopentylmethoxy)benzo[d]thiazol-2-yl)-4-(((1S,2S)-2-(dimethylamino)cyclohexyl)amino)-2-fluorobenzenesulfonamide**

A solution of *N*-(6-(cyclopentylmethoxy)benzo[d]thiazol-2-yl)-*N*-(2,4-dimethoxybenzyl)-4-(((1*S*,2*S*)-2-(dimethylamino)cyclohexyl)amino)-2-fluorobenzenesulfonamide (60 mg, 0.08 mmol) in HCOOH (3 mL) was stirred at room temperature for 16 h. The mixture was concentrated in vacuo and the crude residue was purified by reverse phase chromatography (acetonitrile 35 - 65% / 0.2% HCOOH in water) to afford the title compound (2 mg, 4%) as a white solid

$^1$H NMR (400 MHz, DMSO-$d_6$) δ 7.49 (t, $J$ = 8.8 Hz, 1H), 7.26 (d, $J$ = 2.4 Hz, 1H), 7.16 (d, $J$ = 8.8 Hz, 1H), 6.84 - 6.81 (m, 1H), 6.42 - 6.36 (m, 3H), 3.79 (d, $J$ = 6.8 Hz, 2H), 3.47 - 3.40 (m, 1H), 2.82 - 2.75 (m, 1H), 2.42 (s, 6H), 2.33 - 2.24 (m, 1H), 2.02 - 1.92 (m, 2H), 1.79 - 1.71 (m, 3H), 1.61 - 1.48 (m, 5H), 1.34 - 1.20 (m, 6H).
HRMS (ESI) m/z: 547.2196 $[M+H]^+$

**Compound 5**

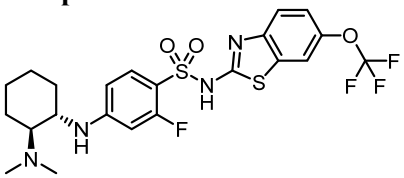

**4-(((1S,2S)-2-(dimethylamino)cyclohexyl)amino)-2-fluoro-N-(6-(trifluoromethoxy)benzo[d]thiazol-2-yl)benzenesulfonamide**

Following the procedure described in compound **6** and replacing 4-(cyclopentylmethoxy)aniline with 4-(trifluoromethoxy)aniline, the title compound was obtained as a white solid.

$^1$H NMR (400 MHz, DMSO-$d_6$) δ 7.64 (m, 1H), 7.52 (m, 1H), 7.30 (d, $J$ = 8.8 Hz, 1H), 7.11 (m, 1H), 6.44-6.37 (m, 3 H), 3.68 (m, 1H), 3.06 (m, 1H), 2.60 (s, 6 H), 2.00 (m, 2H), 1.79 (m, 1H), 1.61 (m, 1H), 1.40- 1.14 (m, 4 H).
HRMS (ESI) m/z: 533.1286 $[M+H]^+$.

231

232 **Supplementary Figure Legends:**

233 **Supplementary Figure 2: (A)** VSD4-$Na_V$1.7-$Na_V$Pas channel protein expression and purification
234 scheme **(B)** Example size exclusion chromatogram and SDS-PAGE of nanodisc-reconstituted VSD4-
235 $Na_V$1.7-$Na_V$Pas channel sample.

236 **Supplementary Figure 3: (A)** Example cryo-EM micrograph image of the VSD4-$Na_V$1.7-$Na_V$Pas
237 channel. **(B)** Representative 2D-class averages of selected particles. **(C)** Data collection and processing
238 workflow for VSD4-$Na_V$1.7-$Na_V$Pas channel bound to compound **4**. **(D)** Heat map representation of the
239 distribution of assigned particle orientations. **(E)** FSC between two half datasets yields a global
240 resolution estimate of approximately 2.2 Å resolution from the refinement using an overall mask of the
241 VSD4-$Na_V$1.7-$Na_V$Pas channel bound to compound **4 (F)** Local resolution of maps. **(G)** Data collection
242 and processing workflow for VSD4-$Na_V$1.7-$Na_V$Pas channel bound to **GDC-0310**. **(H)** Heat map
243 representation of the distribution of assigned particle orientations. **(I)** FSC between two half datasets
244 yields a global resolution estimate of approximately 2.5 Å resolution from the refinement using an
245 overall mask of the VSD4-$Na_V$1.7-$Na_V$Pas channel bound to **GDC-0310**. **(J)** Local resolution of maps.

246 **Supplementary Figure 4: (A)** Data collection and processing workflow for VSD4-$Na_V$1.7-$Na_V$Pas
247 channel bound to compound **2**. **(B)** Heat map representation of the distribution of assigned particle
248 orientations. **(C)** FSC between two half datasets yields a global resolution estimate of approximately 2.9
249 Å resolution from the refinement using an overall mask of the VSD4-$Na_V$1.7-$Na_V$Pas channel bound to
250 compound **2 (D)** Local resolution of maps. **(E)** Data collection and processing workflow for VSD4-
251 $Na_V$1.7-$Na_V$Pas channel bound to compound **2**. **(F)** Heat map representation of the distribution of
252 assigned particle orientations. **(G)** FSC between two half datasets yields a global resolution estimate of
253 approximately 2.5 Å resolution from the refinement using an overall mask of the VSD4-$Na_V$1.7-$Na_V$Pas
254 channel bound to compound **2**. **(H)** Local resolution of maps.

255 **Supplementary Figure 5: (A)** The cryoEM map surrounding the ligand compound **2** is shown in mesh
256 representation. **(B)** The cryoEM map surrounding the ligand compound **4** is shown in mesh
257 representation.

258

259

HPLC chromatogram of compound **2**

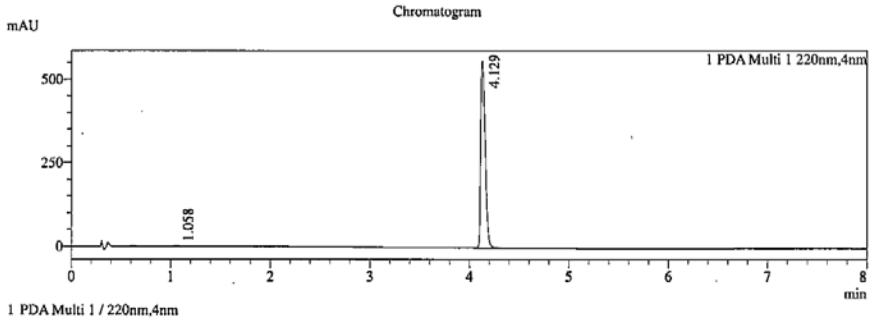


Integration Result

Peak Table

PDA Ch1 220nm

| Peak# | Ret. Time | Height | Height% | USP Width | Area | Area% |
|---|---|---|---|---|---|---|
| 1 | 1.058 | 2105 | 0.384 | 0.071 | 6000 | 0.342 |
| 2 | 4.129 | 546761 | 99.616 | 0.084 | 1750524 | 99.658 |

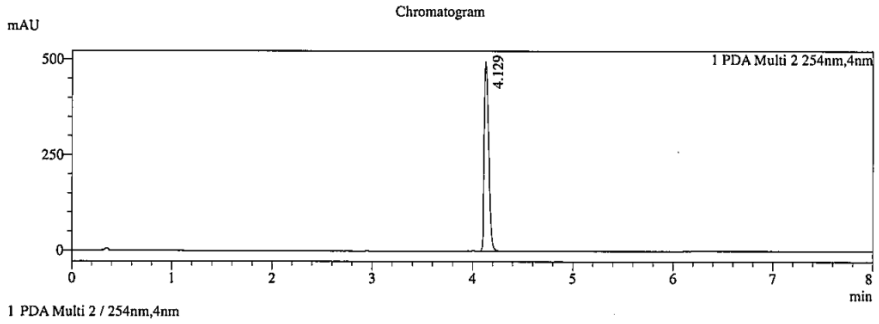


Integration Result

Peak Table

PDA Ch2 254nm

| Peak# | Ret. Time | Height | Height% | USP Width | Area | Area% |
|---|---|---|---|---|---|---|
| 1 | 4.129 | 484289 | 100.000 | 0.084 | 1542826 | 100.000 |

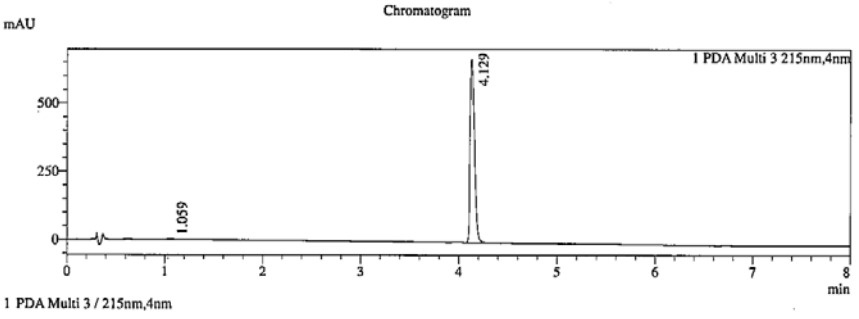


Integration Result

Peak Table

PDA Ch3 215nm

| Peak# | Ret. Time | Height | Height% | USP Width | Area | Area% |
|---|---|---|---|---|---|---|
| 1 | 1.059 | 3033 | 0.461 | 0.071 | 8450 | 0.401 |
| 2 | 4.129 | 655545 | 99.539 | 0.084 | 2099153 | 99.599 |

HPLC chromatogram of compound **3**

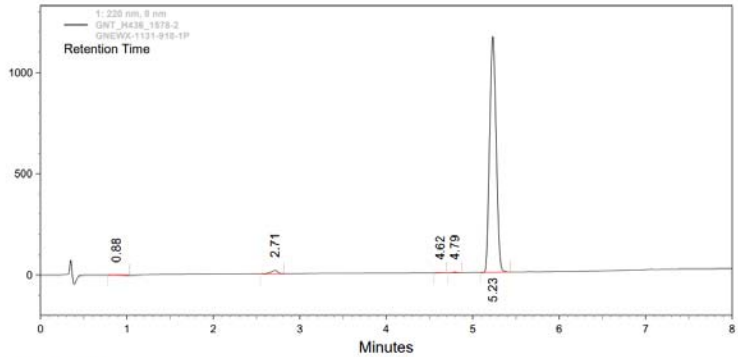


***1: 220 nm, 8 nm***

| *Retention Time* | *Height* | *Area* | *Area Percent* |
|---|---|---|---|
| 0.88 | 2006 | 14264 | 0.23 |
| 2.71 | 17825 | 94685 | 1.52 |
| 4.62 | 1574 | 5119 | 0.08 |
| 4.79 | 4288 | 13870 | 0.22 |
| 5.23 | 1156786 | 6087427 | 97.94 |

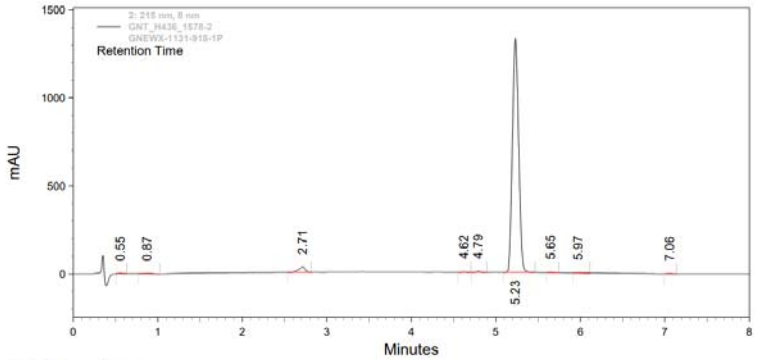


***2: 215 nm, 8 nm***

| *Retention Time* | *Height* | *Area* | *Area Percent* |
|---|---|---|---|
| 0.55 | 3225 | 12600 | 0.18 |
| 0.87 | 3232 | 23433 | 0.33 |
| 2.71 | 29397 | 156299 | 2.23 |
| 4.62 | 2484 | 7826 | 0.11 |
| 4.79 | 4768 | 15348 | 0.22 |
| 5.23 | 1320766 | 6789788 | 96.69 |
| 5.65 | 1640 | 5918 | 0.08 |
| 5.97 | 1527 | 5675 | 0.08 |
| 7.06 | 1670 | 5605 | 0.08 |

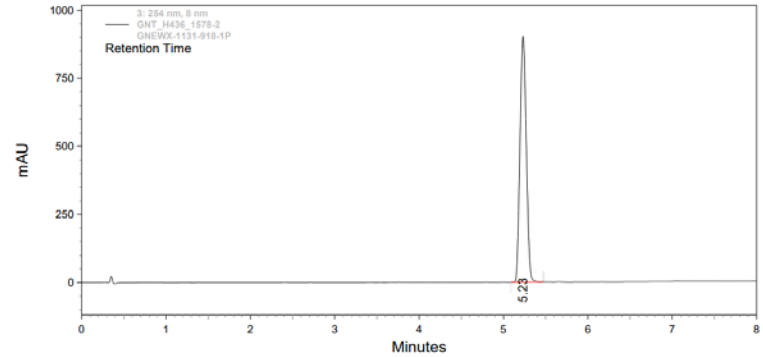


***3: 254 nm, 8 nm***

| *Retention Time* | *Height* | *Area* | *Area Percent* |
|---|---|---|---|
| 5.23 | 897527 | 4692528 | 100.00 |

HPLC chromatogram of compound **4**

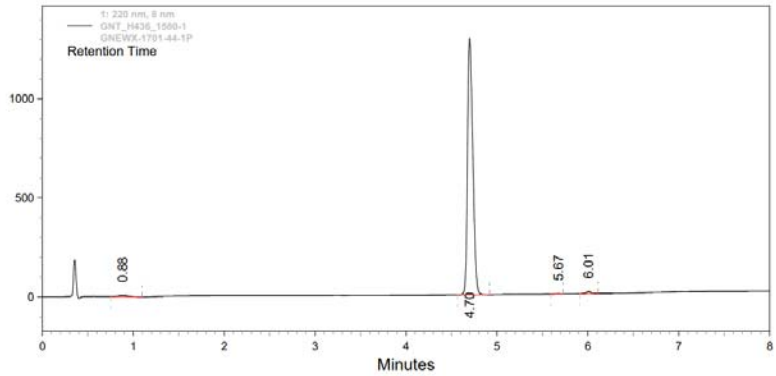


***1: 220 nm, 8 nm***

| *Retention Time* | *Height* | *Area* | *Area Percent* |
|---|---|---|---|
| 0.88 | 5778 | 48393 | 0.91 |
| 4.70 | 1288689 | 5232399 | 98.25 |
| 5.67 | 1644 | 5558 | 0.10 |
| 6.01 | 10759 | 39356 | 0.74 |

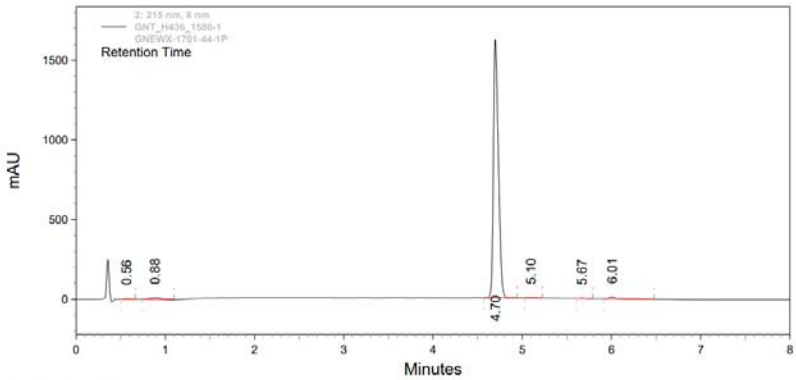


***2: 215 nm, 8 nm***

| *Retention Time* | *Height* | *Area* | *Area Percent* |
|---|---|---|---|
| 0.56 | 2946 | 9287 | 0.14 |
| 0.88 | 9264 | 78075 | 1.22 |
| 4.70 | 1604066 | 6253624 | 97.59 |
| 5.10 | 1747 | 8500 | 0.13 |
| 5.67 | 1685 | 5554 | 0.09 |
| 6.01 | 11358 | 52842 | 0.82 |

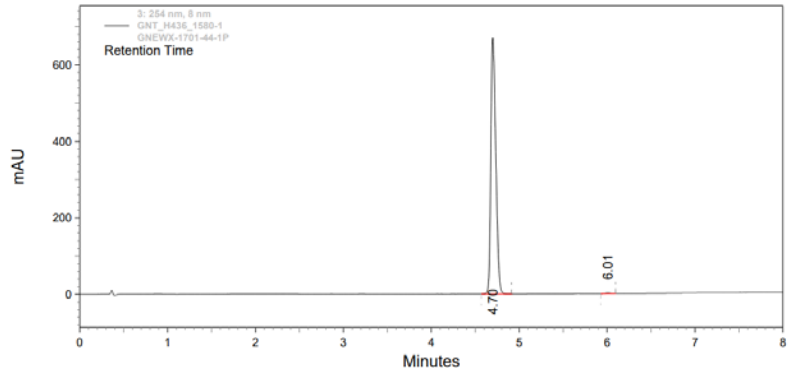


***3: 254 nm, 8 nm***

| *Retention Time* | *Height* | *Area* | *Area Percent* |
|---|---|---|---|
| 4.70 | 665091 | 2626651 | 99.73 |
| 6.01 | 1968 | 7007 | 0.27 |

HPLC chromatogram of compound **5**

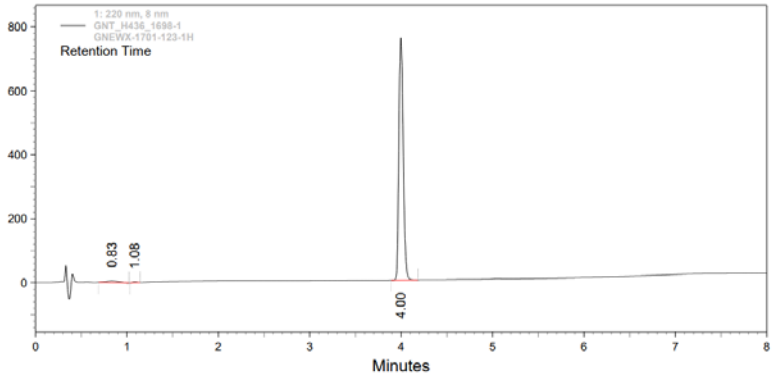


***1: 220 nm, 8 nm***

| *Retention Time* | *Height* | *Area* | *Area Percent* |
|---|---|---|---|
| 0.83 | 5245 | 47427 | 1.85 |
| 1.08 | 2110 | 6804 | 0.27 |
| 4.00 | 753425 | 2510118 | 97.89 |

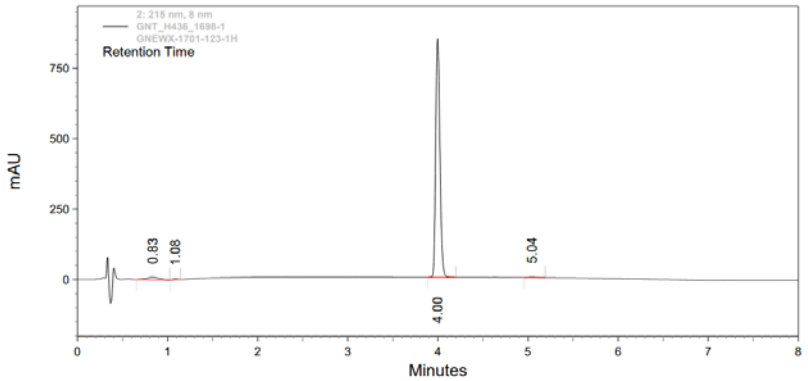


***2: 215 nm, 8 nm***

| *Retention Time* | *Height* | *Area* | *Area Percent* |
|---|---|---|---|
| 0.83 | 8794 | 83696 | 2.90 |
| 1.08 | 3010 | 9655 | 0.33 |
| 4.00 | 842279 | 2784306 | 96.38 |
| 5.04 | 1857 | 11275 | 0.39 |

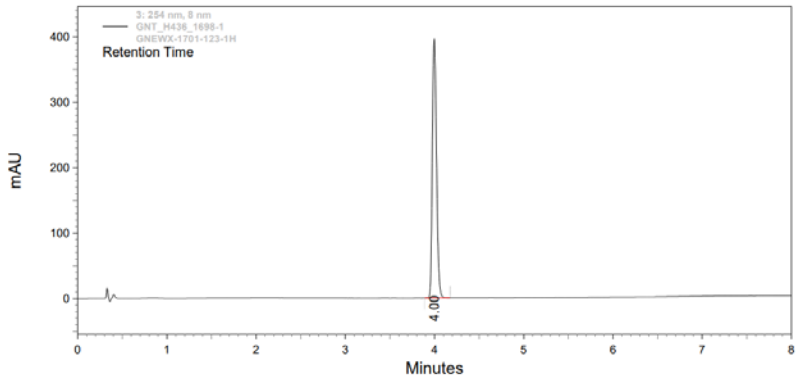


***3: 254 nm, 8 nm***

| *Retention Time* | *Height* | *Area* | *Area Percent* |
|---|---|---|---|
| 4.00 | 393524 | 1296194 | 100.00 |

# Figure 1

change color of linker and of S5

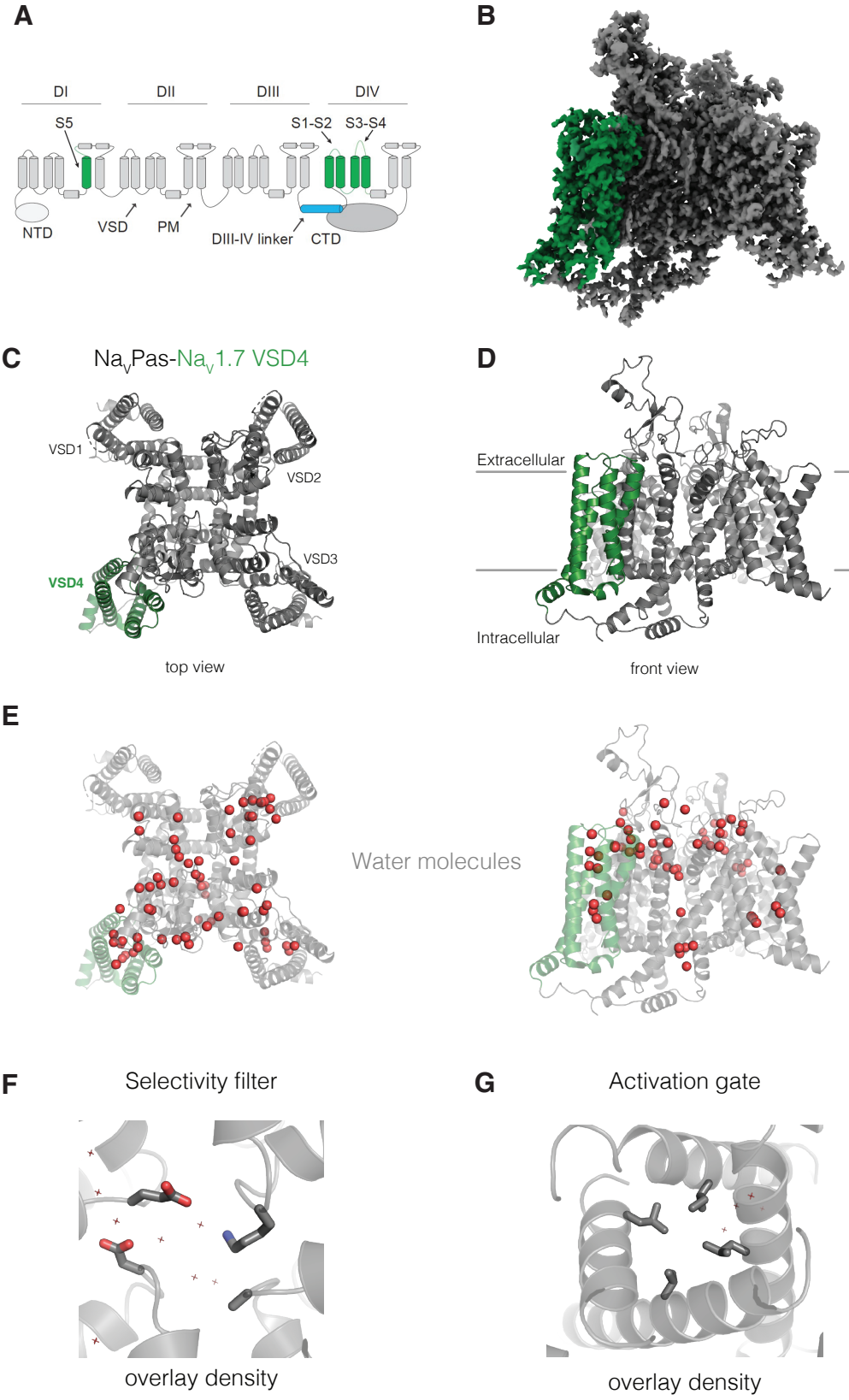

# Figure 2

should we highlight the warhead?

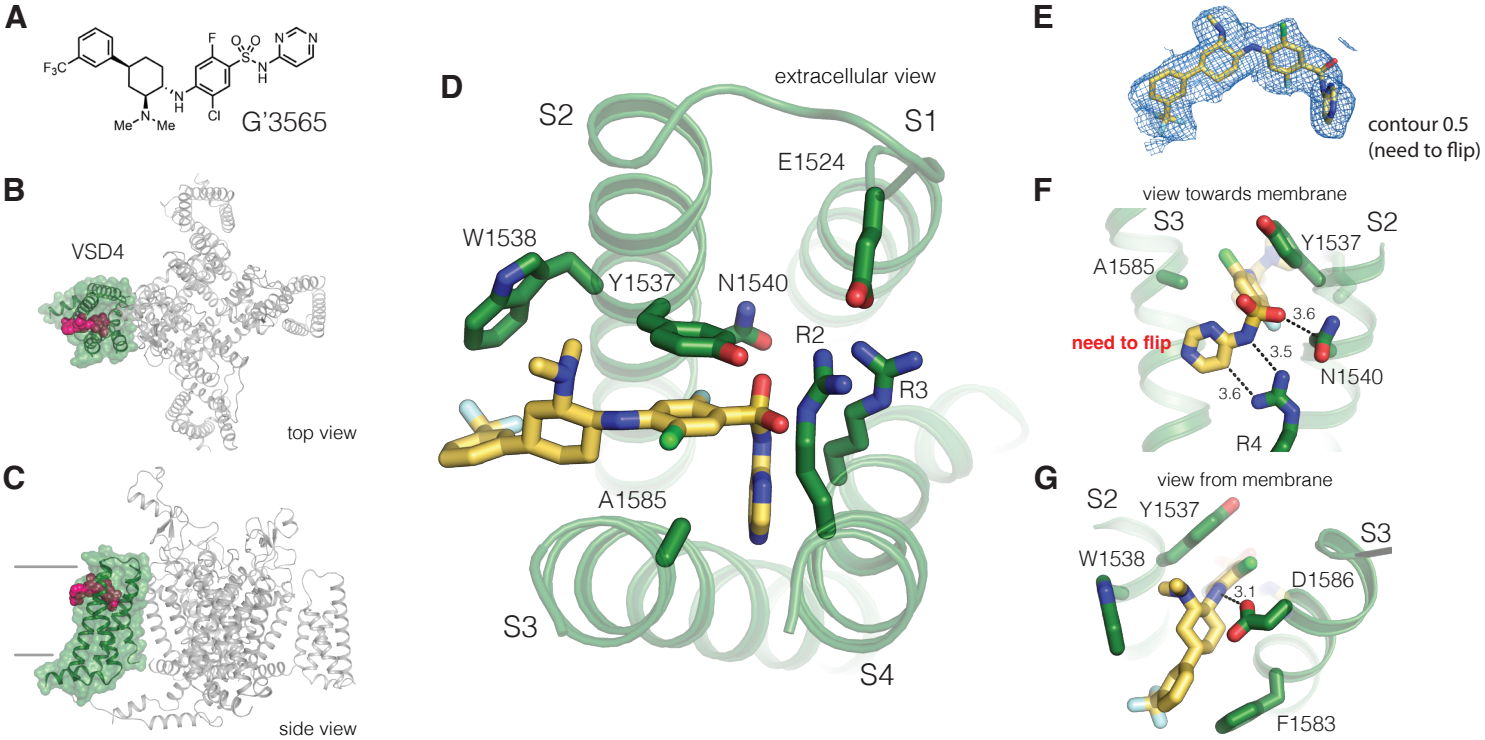

# Figure 3

What numbering should we use (Nav1.7 or from the cosntruct)
the current one doesn't match either case?

should we highlight the warhead?

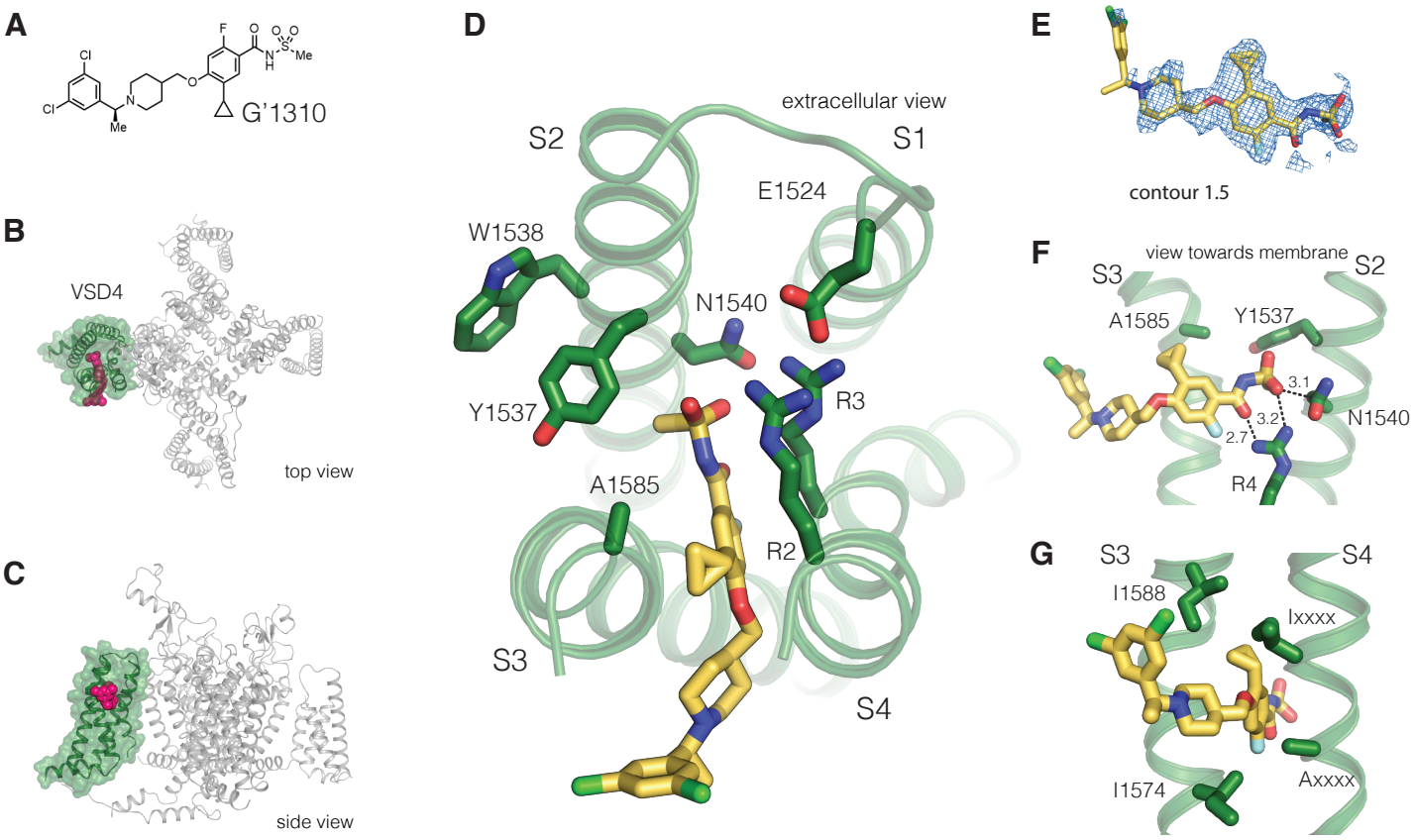

# Figure 4

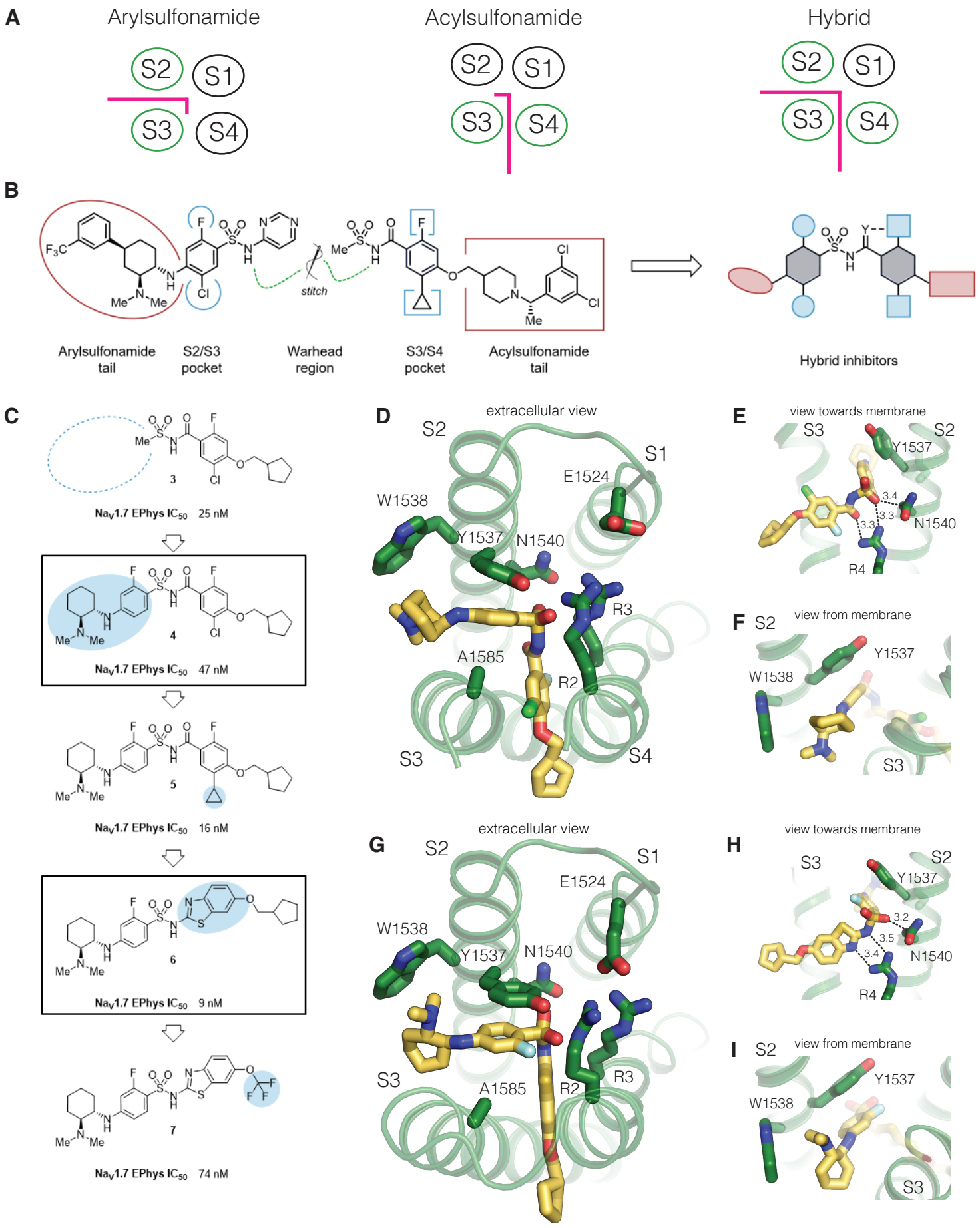
A
Arylsulfonamide
Acylsulfonamide
Hybrid
S2
S1
S3
S4
B
stitch
Arylsulfonamide tail
S2/S3 pocket
Warhead region
S3/S4 pocket
Acylsulfonamide tail
Hybrid inhibitors
C
3
Nav1.7 EPhys IC50 25 nM
4
Nav1.7 EPhys IC50 47 nM
5
Nav1.7 EPhys IC50 16 nM
6
Nav1.7 EPhys IC50 9 nM
7
Nav1.7 EPhys IC50 74 nM
D
extracellular view
S2
S1
E1524
W1538
Y1537
N1540
R3
A1585
R2
S3
S4
E
view towards membrane
S3
S2
Y1537
3.4
3.3
3.3
N1540
R4
F
S2
view from membrane
Y1537
W1538
S3
G
extracellular view
S2
S1
E1524
W1538
Y1537
N1540
S3
A1585
R2
R3
H
view towards membrane
S3
S2
Y1537
3.2
3.5
3.4
N1540
R4
I
S2
view from membrane
Y1537
W1538
S3

# Supplementary Figure 1

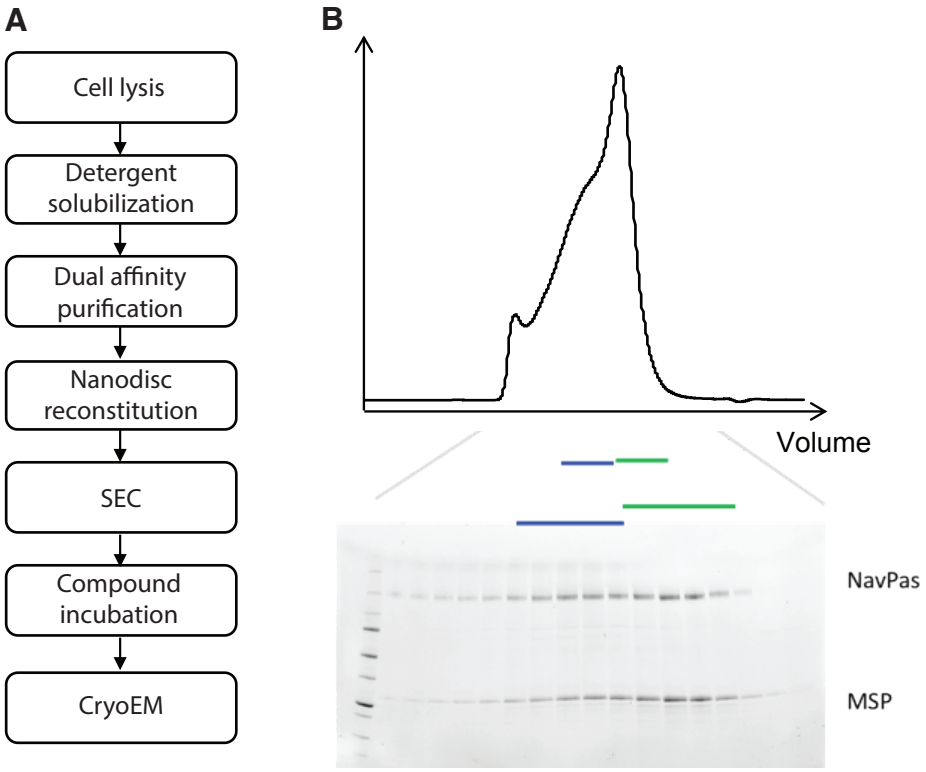

# Supplementary Figure 2

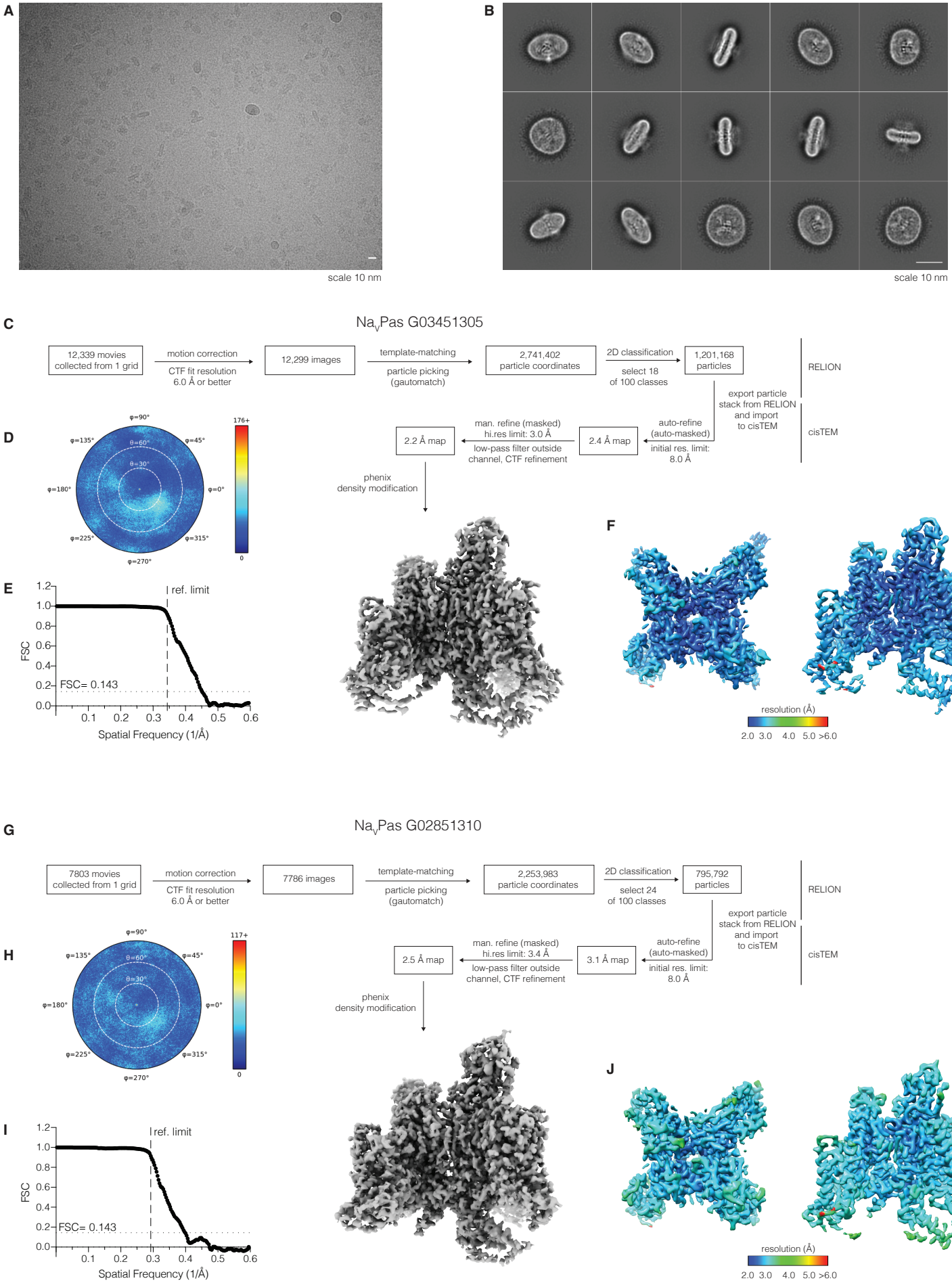

# Supplementary Figure 3

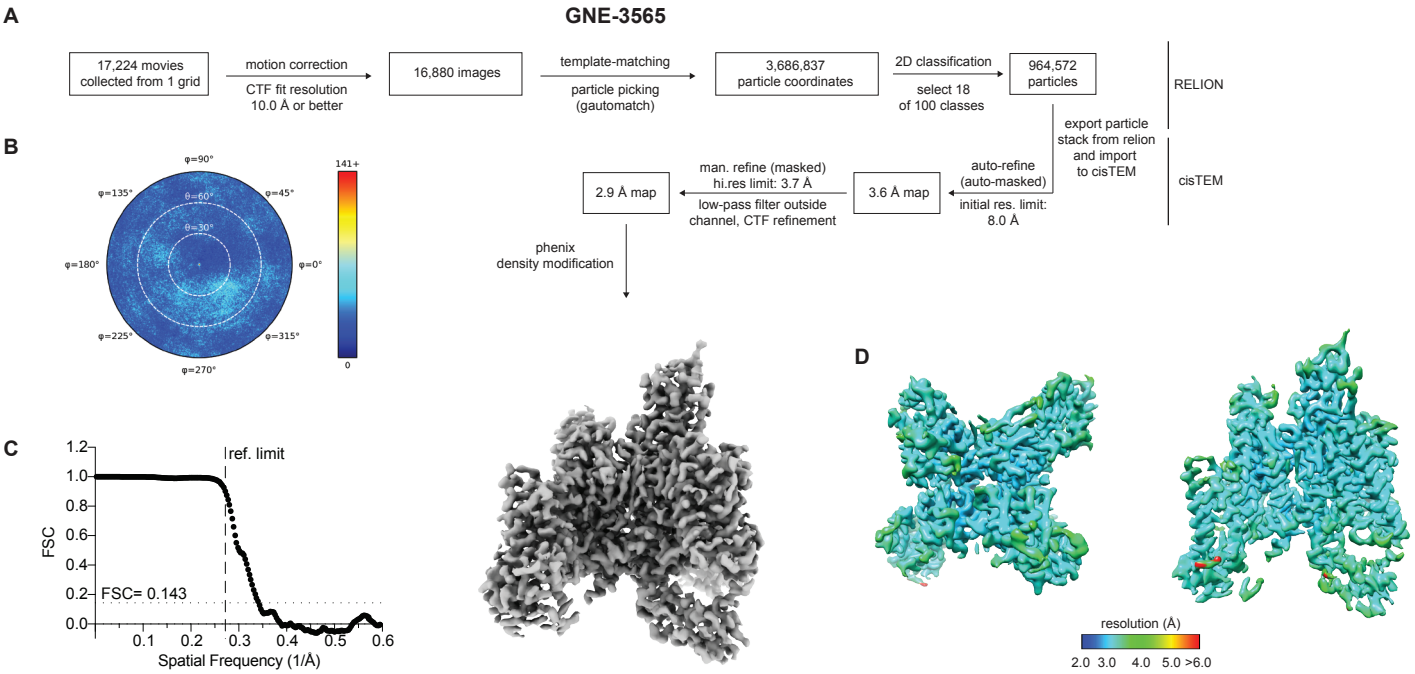


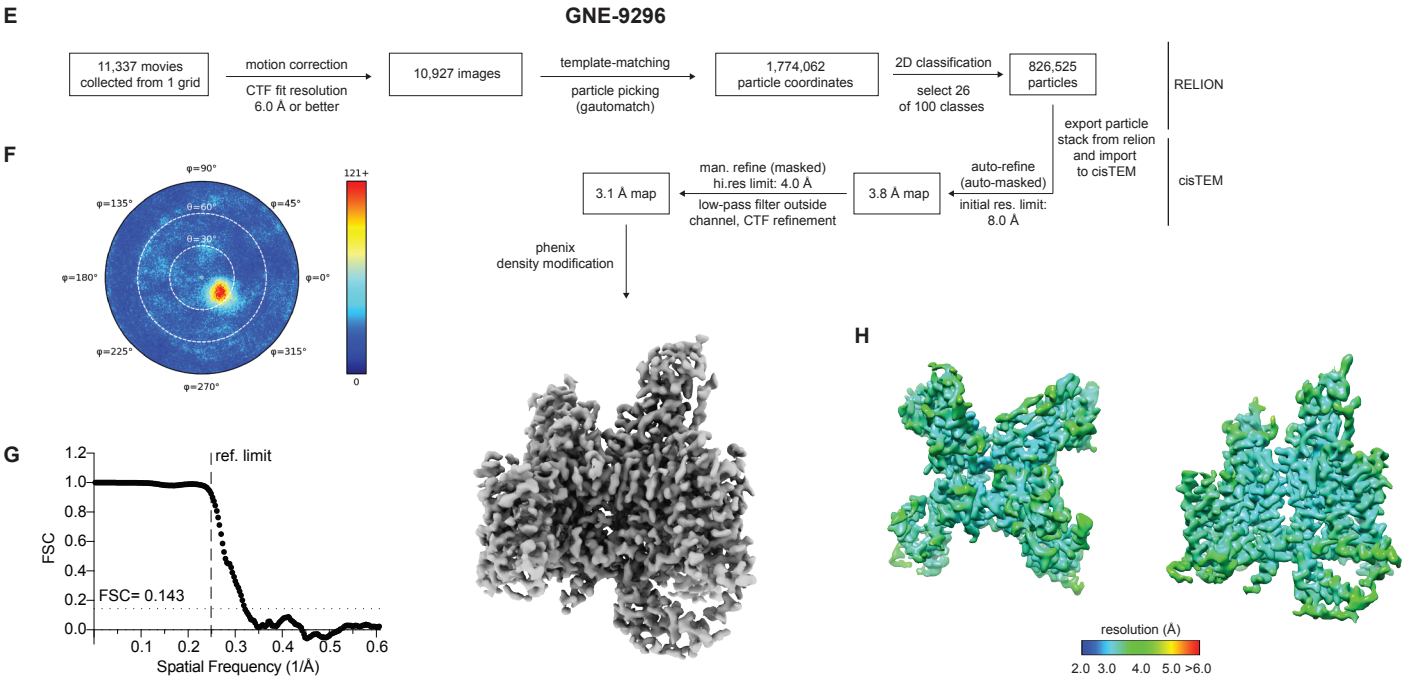
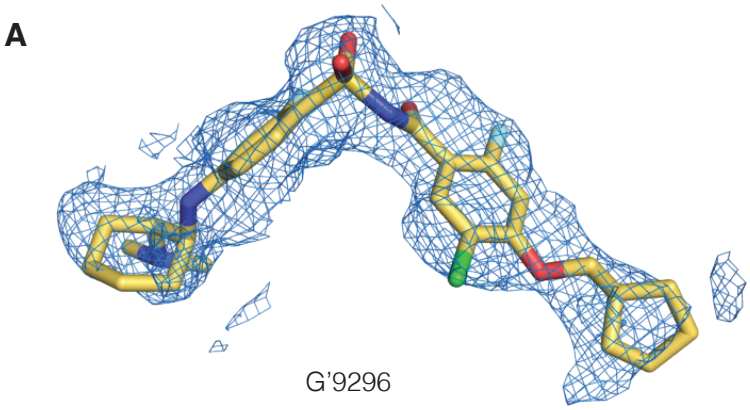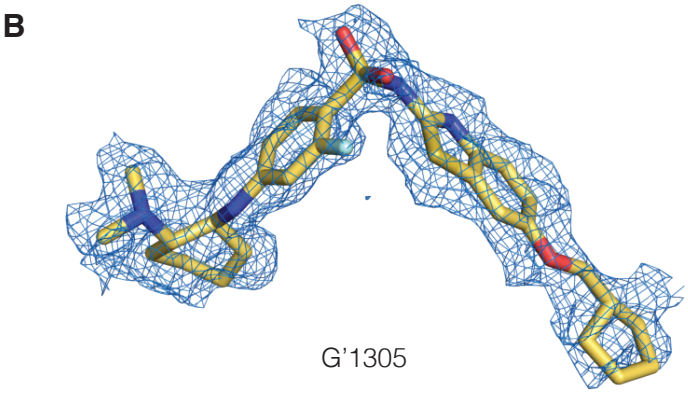
Supplementary Figure 4